OSCCAR:
FUTURE OCCUPANT SAFETY FOR CRASHES IN CARS

Standardised validation procedure for qualifying the HBM to be used for assessing effectiveness of pilot protection principles

Document Type	Deliverable
Document Number	D5.2
Primary Author(s)	Steffen Peldschus, Anja Wagner, Julia Mühlbauer, Laura Riegler, Johanna Kerschreiter | LMU Johan Davidsson | Chalmers Corina Klug | TU Graz Simon Dussinger | ESI Matthias Schießler, Andre Eggers | BASt
Document Version / Status	2.1 | Final
Distribution Level	PU (public)

Project Acronym	OSCCAR
Project Title	FUTURE OCCUPANT SAFETY FOR CRASHES IN CARS
Project Website	www.osccarproject.eu
Project Coordinator	Werner Leitgeb | VIF | werner.leitgeb@v2c2.at
Grant Agreement Number	768947
Date of latest version of Annex I against which the assessment will be made	2021-02-05
Upload by coordinator:	First submitted: 2021-12-20 Re-submitted: 2022-04-11

OSCCAR has received funding from the European Union's Horizon 2020 research and innovation programme under grant agreement No 768947.

CONTRIBUTORS

Name	Organization	Name	Organization
Steffen Peldschus	LMU	Corina Klug	TUG
Anja Wagner	LMU	Andre Berger	ESI
Julia Mühlbauer	LMU	Simon Dussinger	ESI
Laura Rieger	LMU	Krystoffer Mroz	Autoliv
Nikolas Pfeiffer	LMU	Martin Östling	Autoliv
Johanna Kerschreiter	LMU	Richard Lancashire	Siemens
Andre Eggers	BASt	Michael Sprenger	ZF
Johan Davidsson	Chalmers	Matthias Schießler	BASt
Sabine Compigne	TME		

FORMAL REVIEWERS

Name	Organization	Date
Marco Grottoli	SISW	2021-12-10
Cristian Jimenez	IDIADA	2021-12-09

DOCUMENT HISTORY

Revision	Date	Author / Organization	Description
0.1	2021-11-20	AW, JM, LR, NP, JK, SP	Initial draft
1.0	2021-11-30	all	Draft
1.1	2021-12-04	JD, SP	Final draft
2.0	2021-12-11	AW, SP	Final
2.1	2022-04-07	MK	Updates after EU review

TABLE OF CONTENTS

1 EXECUTIVE SUMMARY 7

2 OBJECTIVES 8

3 DESCRIPTION OF WORK 9

3.1 Overview Virtual Testing approach (BASt, LMU) 9

3.1.1 Vehicle environment model validation-based certification procedure 9
3.1.2 Selection of appropriate validation tests and validation device 10
3.1.3 Selection of validation channels 11
3.1.4 Workflow and roles of involved parties in a vehicle environment model certification process 12
3.1.5 Model version control 12
3.1.6 Acceptance criteria for validation-based certification considering test scatter 13
3.1.7 Proposal for acceptance criteria considering scatter in validation test procedure and validation device 13
3.1.8 Proposal how to consider scatter in vehicle component response 14
3.1.9 Application to OSCCAR homolongation test case 15
3.1.10 Validation load cases and validation device for OSCCAR homolongation test case 15
3.1.11 Selection of validation channels 16
3.1.12 Application of the proposed objective acceptance criteria for environment certification 17

3.2 Standardised naming of reference points in HBMs (LMU, TUG, ZF) 19
3.3 Protocols for harmonised reference point identification (LMU) 23

3.3.1 Spine reference points and local coordinate system definition 23
3.3.2 Head reference points based on Frankfort plane 26
3.3.3 Script for automatically calculating hip joint rotation centers based on STLs (H-point) 26

3.4 Volunteer testing protocol (Chalmers, TUG) 30

3.4.1 Ethical considerations 30
3.4.2 Study Design 30
3.4.3 Documentation 31
3.4.4 Measurements 32
3.4.5 Data analysis 33

3.5 Code-specific requirements for pre-processing and post-processing (ESI) 34

3.5.1 Introduction 34
3.5.2 Code specific requirements for pre-processing 34
3.5.3 Element formulations and element mesh 39
3.5.4 Code specific requirements for post-processing 43

3.6 Public load case modelling reclined frontal impact (Autoliv, BASt, ESI, LMU, Siemens) 44

3.6.1 Semi-rigid seat 44
3.6.2 Belt and Retractor 45

3.6.3 Interaction between Belt and HBM, contact algorithms and mesh size 46
3.6.4 Experimental targets 46

4 DISSEMINATION, EXPLOITATION AND STANDARDISATION 47

5 CONCLUSIONS 48

6 REFERENCES 49

A. APPENDIX – NAMING CONVENTION 50

LIST OF FIGURES

Figure 1 Flowchart OSCCAR HBM-based virtual testing procedure 9

Figure 2 50-percentile female neck model (Source: Östh et al., IRCOBI 2017 [2]) 11

Figure 3 Validation device 50-percentile female rear impact seat evaluation tool VIVA II (Source: http://crashscene.se/f50flogard) 11

Figure 4 Proposal how to consider scatter in vehicle components in VT with exemplary upper and lower parameter values 15

Figure 5 OSCCAR homologation demonstrator 16

Figure 6 Sled test setup with THOR-50M in reclined seating position (Thorax angle: 48°) 16

Figure 7 Channels were considered suitable and relevant 16

Figure 8 Channels failing the 1st stage of the objective acceptance criteria 17

Figure 9 Anatomical orientations and wording 19

Figure 10 Naming convention 20

Figure 11 Illustraion of the fill-up algorithm and examples 21

Figure 12 Midplane construction by averaging the planes fitted to the upper and lower vertebral endplates 24

Figure 13 Input nodes for calculation of center of canal ring (c_{cr}) 25

Figure 14 Local coordinate system in midplane with x defined through center points of spinal canal (c_{cr}) and vertebral body (c_{vb}) 25

Figure 15 Local spine coordinate system in THUMS 4.2 (L1-L5) 25

Figure 16 Defining the h-point (red) as midpoint of the hip joint rotation centers (yellow) which are defined as centroids of acetabulum nodes 27

Figure 17 Flowchart of method for automatic calcualtion of hip joint rotation centers based on an input STL of the acetabulum region (method developed by Nikolas Pfeiffer, LMU [11]) 28

Figure 18 steps of automatic identification of acetabulum border triangles and hip joint rotation center calculation a) imported STL with triangle normal; b) acetabulum border triangles identified by k means algorithm (blue); c) circle fitted with Kasa method (red) and circle normal (black); d) acetabulum triangles for joint rotation center and H-Point calculations 29

Figure 19 Rope friction test case for comparison of edge friction behavior between LS Dyna and VPS 36

Figure 20 Curves for force and displacement loading at belt ends 36

Figure 21 Belt routing, belt forces $\boldsymbol{F1}$, $\boldsymbol{F2}$ and opening angle $\boldsymbol{\beta}$ 37

Figure 22 coarse and warped versus fine and even cylinder mesh (left: VPS, right: LS Dyna) 37

Figure 23 Loss of friction force in LS Dyna with coarse and warped cylinder mesh 38

Figure 24 Improved belt force in LS Dyna for a fine and even cylinder mesh 39

Figure 25 Single element test cases for material calibration 40

Figure 26 Example *MAT_ELASTIC, shell element (UI) 40

Figure 27 Comparison results LS-DYNA (green) vs. VPS (red) for single element testing for pure elastic material represented by SHELL elements 41

Figure 28 Example *MAT_LOW_DENSITY_FOAM, solid element (SRI) 41

Figure 29 Comparison results LS-DYNA (green) vs. VPS (red) for single element testing for foam material represented by SOLID elements 42

Figure 30 Scheme to minimize unphysical numerical scatter 42

Figure 31 Example for unfavorable definition of material curves with respect to numerical scattering 43

Figure 32 Global energy plot example 44

LIST OF TABLES

Table 1 List of functional locations for the spine, the ribs and the head 22

Table 2 Spine reference points provided to OSCCAR consortium 26

Table 3 head reference points provided to OSCCAR consortium 26

Table 4 Hip joint reference points 27

Table 5 Mechanical design and specifications of the semi-rigid seat as used in different projects. 45

Table 6 Common head landmarks and corresponding code according to Naming Convention 51

Table 7 Common upper body landmarks and corresponding code according to naming convention 53

Table 8 Common upper extremity landmarks and corresponding code according to naming convention 56

Table 9 Common cervical spine landmarks and corresponding code according to naming convention 62

Table 10 Common thoracal spine landmarks and corresponding code according to naming convention 75

Table 11 Common lumbar spine landmarks and corresponding code according to naming convention 79

Table 12 Common landmarks of the lower extremities and corresponding code according to naming convention 83

Table 13 Common landmarks of the pelvis and corresponding code according to naming convention 85

1 EXECUTIVE SUMMARY

This report summarises the findings from activities related to the preparation and pre-processing of Virtual Testing (VT) with Human Body Models (HBMs).

Virtual Testing with HBMs incorporates a structured process of model development, the action of admitting a model, and the actual virtual test leading to an assessment. These three phases, building on the definitions from the IMVITER project, are applied to all involved models - HBM as well as models of the included elements of the vehicle.

The decision whether an HBM is admitted to a third (final) phase of VT can be described as certification process. This includes the definition of requirements such as validation and comparability as needed for the specific VT scenario. For this phase, validation load cases and comparability load cases need to be modelled in several crash codes, for which recommendations were made in this report.

HBMs need further attendance in terms of validation for new seating positions associated to automated driving. The first available set of data in this context of full-scale experiments has been addressed in OSCCAR. Modelling of those experiments has been addressed with the objective of providing publicly available simulation elements.

Apart from new seating positions, the automation also increases the importance of the pre-crash phase. Modelling the occupant in this phase is usually tackled by active HBMs. For their validation, volunteer test data is needed. Recommendations on the acquisition of such data are given in this report.

Pre-processing HBMs in a VT application will require the definition of size (anthropometry) and position, for which reference points are needed. The identification of such points on different HBMs in an unambiguous way is challenging. It was therefore demonstrated in this report how such points and related orientations (coordinate systems) can be defined. In order to facilitate a standardised communication on the points, an extensive list of names based on system compatible with existing naming approaches was created.

Within a process of involving an HBM and vehicle elements (as for instance in a virtual sled test), simulation results including risk-curve based assessment will need to consider scatter from different sources. A procedure how this can be defined beforehand, is included in this deliverable.

2 OBJECTIVES

This report aims at summarising activities related to the preparation and pre-processing of Virtual Testing with Human Body models from the OSCCAR project and deriving recommendations that can serve as a basis for future VT related activities and implementation in regulatory or consumer testing.

The aspects addressed with the ambition of formulating recommendations include admitting and using HBMs in VT procedures, including the question on how considerations of scatter, which are required by the particularity of vehicle model handling in VT, influence the HBM calculations.

HBMs need further attendance in terms of validation for new seating positions associated to automated driving. Providing elements for modelling the first available full-scale test data in this context was addressed within OSCCAR. Recommendations were also targeted for the increasingly important volunteer testing aiming at validation of active HBMs.

With the work summarised in this report, contributions were to be made to standardisation and harmonisation of pre-processing procedures of HBMs in terms of definitions of reference points or landmarks and in terms of naming such points.

3 DESCRIPTION OF WORK

3.1 Overview Virtual Testing approach (BASt, LMU)

This report describes elements of a Virtual Testing procedure using HBMs. Within task 5.1, a validation procedure was developed considering the results from the EU project IMVITER (https://cordis.europa.eu/project/id/218688) . This procedure is outlined in a flowchart consisting of three phases. A first version was shown in OSCCAR D5.1 [1]. Based on expert workshops and application of the procedure to pilot cases a refined updated version of this was procedure developed shown in Figure 1.

This procedure is outlined in a flowchart consisting of three phases:

1. Phase 1: Development of the vehicle environment simulation model, done by the vehicle manufacturer
2. Phase 2: An official validation procedure to demonstrate that the environment model correctly represents the real vehicle
3. Phase 3: A new VT based homolongation (or assessment) load case including an HBM suitable and certified for this new load case

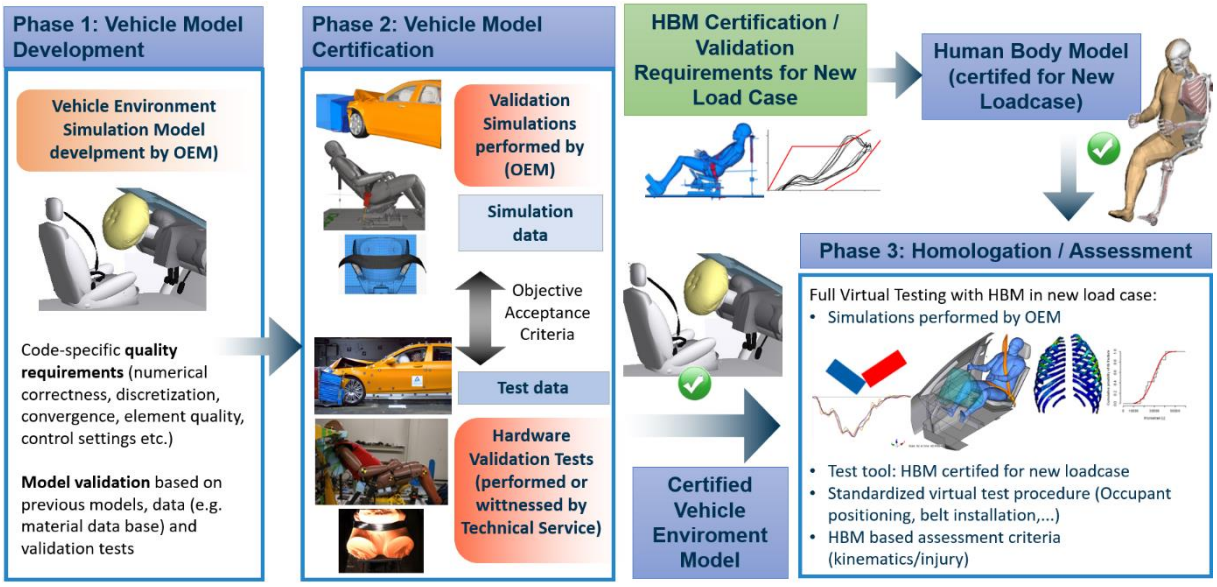

Figure 1 Flowchart OSCCAR HBM-based virtual testing procedure

In the following sections more detailed explanations will be provided regarding the necessary elements of phase 2, the vehicle environment model validation, which needs to be fulfilled before the model can be admitted to HBM-based VT.

3.1.1 Vehicle environment model validation-based certification procedure

To choose the appropriate validation load cases for phase 2 including the validation device a detailed review of the new load case defined in phase 3 should be the starting point. It should also be

considered which safety systems or restraint concepts will be motivated or adapted in the case of the new requirements defined in Phase 3. New safety concepts might result in different interaction of the HBM with the vehicle environment which have to be considered for the definition of validation tests.

3.1.2 Selection of appropriate validation tests and validation device

The objective of the validation tests is to prove (within an official process opened after Phase 1) the validation of all components of the vehicle environment interacting with the occupants in the new load case. For these components, key focus should be given on the body regions and phenomena that are most relevant for the injury assessment.

To validate the vehicle environment, the components of the vehicle environment should be loaded in a similar way as by the HBM in the assessment or homologation load case. To enable this, a Validation Device (VD) is needed that represents the loading as similar as possible to the HBM. The applicability of a standard ATDs as validation device might be questionable as they are not designed for these new load cases.

The general requirements for a VD are listed below:

- Representative resulting loading between vehicle environment and HBM in the new assessment load case (including possible new restraint concepts), which is to be achieved most easily by the VD incorporating:
  - In terms of anthropometry as similar as possible to the occupant represented by the HBM in the new load case
  - In the new load case realistic human-like (HBM-like) occupant kinematics considering the principal direction of loading (e.g. front, side, rear, ...)
- Robust, repeatable, reproducible, re-usable in real testing
- Corresponding CAE model applicable in new (validation) load case

For more complex load cases involving new assessment criteria, a new VD more representative of the HBM in terms of shape and kinematics in the relevant loading conditions might be needed. An example for this, is a VD developed within the VIVA II project [2]. To validate a seat model to be evaluated with a 50-percentile female HBM (Figure 2) no corresponding rear impact validation device in terms of using a standard ATD is available. All available rear impact dummies for real testing are representing an average male occupant. For a new HBM-based VT procedure with a 50-percentile female HBM a new VD (Figure 3) whose design focusses on the interaction between test tool and the seat could be used for validation of the vehicle environment simulation model.

Figure 2 50-percentile female neck model (Source: Östh et al., IRCOBI 2017 [2])

Figure 3 Validation device 50-percentile female rear impact seat evaluation tool VIVA II (Source: http://crashscene.se/f50flogard)

3.1.3 Selection of validation channels

The objective of the extended model validation is to ensure the virtual components (e.g. belt, airbag, interior trims) are loading the HBM in the correct way reflecting the loading and interaction with the HBM like the real vehicle components. Thus, the relevant validation measurements that have to be compared between test and simulation should be in the first place the loads (e.g. belt loads) acting between these components and the occupant. Also, more advanced measurements like pressure distribution between the validation device and the vehicle components could be considered in the future for a more robust validation.

By the validation procedure it has to be assured that the interaction between occupant and restraint (e.g. belt sliding) and resulting load distribution within the occupant is correct. For this purpose, the following measurement might also be needed in the validation procedure:

- internal ATD measurements (e.g. IR-TRACCS, clavicle loads)
- tracking of belt movement
- load / pressure distribution measurements

The focus should be placed on the body regions that will be of main interest for the HBM-based injury assessment. Body regions that are not used for the HBM-based injury assessment should also be considered, but only with the focus of correct load transmission.

Furthermore, kinematic measurements should be considered, if it is feasible to take the measurements during the test. If possible, target tracking should be evaluated. Alternatively, the whole-body kinematics could also be assessed by the accelerations of relevant body parts.

For each selected validation device and validation channel, it can be discussed if only the relevant loading direction or resultant has to be considered. For example, in a frontal impact load case only some of the x-direction ATD signals might be relevant whereas in an oblique load case also the lateral direction of ATD signals might have to be considered.

3.1.4 Workflow and roles of involved parties in a vehicle environment model certification process

The objective of the certification procedure (Phase 2) as shown in Figure 1 is to ensure that the simulation model of the vehicle environment is sufficiently validated to be used for VT with a human body model in the new load case. To ensure a similar level of trust in the whole VT procedure compared to a real testing-based procedure the definition of a clear work flow and responsibilities of the involved parties is necessary.

Option A: A very strict procedure would follow these steps in sequential order:

1.) The OEM sets up and subsequently improves the simulation model also by calibrating to internal hardware tests on sled and component level up to a status that it is sufficiently validated to be used for Virtual Testing. At this stage the model status must be frozen. It has to be assured that exactly this version of model will later be also used in the homologation/assessment simulation (Phase 3). With this model all defined validation load cases should be carried out by the OEM with the simulation model. The detailed simulation results for all validation load cases should be provided in an agreed data format. Together with the data a report could be provided to show the level of validation.

2.) In a next step a technical service or an accredited consumer testing lab would carry out all or selected hardware validation tests. Another option could be witnessed tests, which are carried out by the OEM or an accredited lab.

3.) In a third step, based on an objective acceptance procedure, the validation status of the vehicle environment model should be confirmed by clearly defined criteria. After that the environment model can be labelled by a consumer testing organization (NCAP) or technical service/type approval authority as certified for use in Phase 3 of the VT procedure.

If boundary conditions (e.g. dummy position or crash pulse) differ significantly between simulation and hardware testing, the validation simulations with adjusted boundary condition might be repeated. However, it has to be assured that the vehicle model itself is not changed.

Option B: To reduce the effort for the consumer testing organization/technical service/type approval authority and to simplify the procedure, it could also be proposed to certify the vehicle environment model based on a validation report summarizing the internal validation work done by the OEM during the vehicle model development (Phase 1). In Phase 2 the technical service or expert at a consumer testing organization would check the validation report and confirm the certification of the model for VT testing based on the report. Technically, this is somewhat comparable to what is called self-certification in the sphere of responsibility of NHTSA. However, this procedure would allow less credibility and trust compared to the previously described approach.

Possible Option C is also to go for Option B in general, but on a case by case decision keep open the possibility to carry out validation tests by the technical service or consumer testing lab (as described in Option A) to confirm the results presented in a validation report. However, for this approach also clear pass or fail criteria would be needed.

3.1.5 Model version control

Currently (following the IMVITER proposal and Euro NCAP approach) the vehicle environment model as well as the HBM, will not be shared outside the companies. In this kind of VT process the quality and validity of the models will be checked and finally approved for further use for VT by a certification procedure. For the vehicle model this will be based on a validation testing-based procedure described within this report. After certification of the vehicle model it has to be made sure,

that the same model is used in the whole validation process and eventually for VT-based assessment or type approval.

This can be done or is currently done on a basis of trust and based on OEM internal documentation systems. However, if HBM-based Virtual Testing will be used in a homologation of type approval process also an IT-based level of “labelling” (such as check sum, encryption or similar) might be needed. The models could get a kind of “certified” label and the vehicle manufacturer has to guaranty that exactly this model will be used within the whole virtual consumer test or homologation procedure.

Different options to ensure this requirement should be further investigated. After a model (HBM or vehicle/interior) is certified it could be encrypted or “locked” in a way that it cannot be further modified without permission which might result in a re-certification or update of the certification report. Another option could be that the model receives a unique labelling. All simulation results (output data/plots/reports) which are generated with exactly that model would automatically carry that label. It might be also possible to automatically generate some kind of “hash” code from simulation input file, which is always provided together with outputs/results and reports.

3.1.6 Acceptance criteria for validation-based certification considering test scatter

As explained in the previous section the reliability of the validation procedure in a VT-based homologation process is crucial. Failure within the validation process is no option for the OEM, because there is no VT-based backup option.

This leads to the following requirements for a validation-based certification procedure for a vehicle model to be used in an HBM Virtual Testing process:

- Pass/fail criteria needed to objectively distinguish between valid and a non-valid model
- The criteria should be stringent to assure the correct validation of vehicle environment to guarantee the same level of trust in a full VT procedure like in a RT-based procedure
- At the same time the procedure has to be achievable to make sure it is possible to pass the criteria of the vehicle environment validation with reasonable efforts.

A realistic validation procedure should consider the test scatter. Three main sources of test scatter in validation tests were identified:

1. Scatter in real test procedure (pulse, dummy positioning, belt routing, …)
2. ariation in validation device (hardware dummy variation)
3. Variation in vehicle components

3.1.7 Proposal for acceptance criteria considering scatter in validation test procedure and validation device

R&R (Repeatability and Reproducibility) studies should be used to identify the test scatter that can be expected in a Phase 2 validation test. Thereby, for each validation channel, the reproducibility should be calculated based on an objective evaluation methodology (e.g. CORA or ISO/TS 18571) and multiple test series, ideally conducted in different laboratories. The rating provided by the objective evaluation methodology of any validation channel comparing the response of the model to one validation test is expected not to be better than the reproducibility (scatter) of the corresponding channel in the hardware test. From this perspective, the reproducibility in the hardware test is the

maximum quality that can be expected from a validation channel. Since this requirement can rarely be fulfilled, adjustment considering the identified scatter should be applied.

Based on the reproducibility and adjustments considering the achievable predictability of the simulation model (-20%), an Objective Acceptance Criterion (OAC) is proposed:

$$OAC_{Channel} = (1 - 0.2) \cdot Reproducability_{Channel}$$

The following two-stage objective acceptance criterion, based on the rating from an objective evaluation methodology (e.g. CORA or ISO/TS 18571) and calculated from the validation simulation and corresponding hardware validation test as reference, is proposed:

1. For acceptance, the objective evaluation value of each validation channel has to be above the previously determined $OAC_{Channel}$

2. Channels that do not fulfil this criterion have to be reviewed

    a) Channels with an objective evaluation value below the $OAC_{Channel}$ but above the threshold of 0.58 might be acceptable. However, justification is necessary.

    b) Channels with an objective evaluation value below the threshold of 0.58 are not acceptable unless detailed justification is provided (e.g. problems in hardware testing, shortcomings in the model of validation device not affecting the interaction of the HBM with the vehicle environment).

3.1.8 Proposal how to consider scatter in vehicle component response

In real testing-based type approval and assessment procedures the vehicle manufacturer takes the vehicle component scatter into account by a robust design including a safety margin with respect to some specific requirements (e.g. ATD injury reference values). Even a vehicle with a worst-case performance of the relevant component would have to fulfil the requirements.

To ensure the same in a full VT procedure, the following process is proposed (see Figure 4). For the simulation of the validation load cases, an upper and a lower setting of relevant vehicle environment component parameters should be used. If in best case available, a distribution of input parameters could be used in a stochastic simulation.

A corridor should be provided based on simulations for (combinations of) upper and lower outputs (or output distribution) of validation channels. The corresponding output channel from the real validation test would not have to match exactly one deterministic simulation output, but be within the corridor to be accepted as validated. The same upper and lower parameters would also have to be used in the vehicle environment model in homologation/assessment simulation (Phase 3).

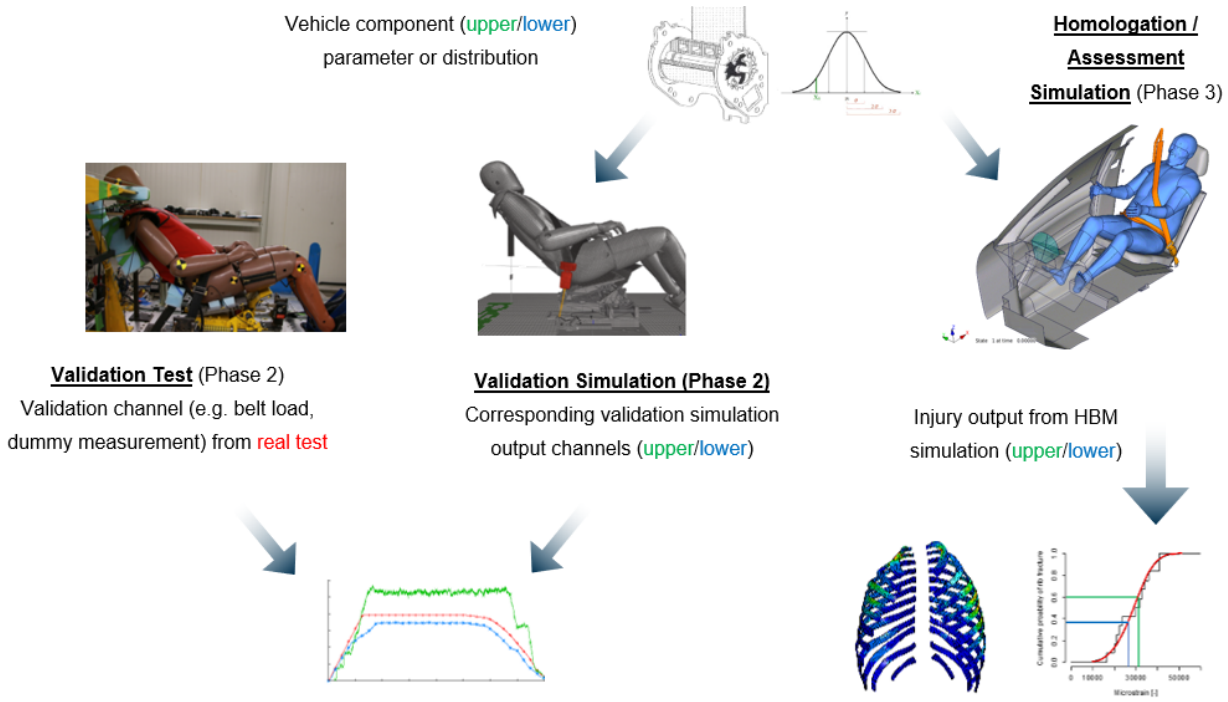

Figure 4 Proposal how to consider scatter in vehicle components in VT with exemplary upper and lower parameter values

3.1.9 Application to OSCCAR homolongation test case

The OSCCAR homologation test case includes a test setup with a highly reclined seating position resulting in a thoracic angle of 48°. The crash configuration is a full-frontal loading direction with a 50 km/h deceleration pulse. For assessment an HBM representing a 50%ile male occupant is used (see Figure 5). CORA [3] with standardized parameters was chosen as objective evaluation methodology.

3.1.10 Validation load cases and validation device for OSCCAR homolongation test case

For the OSCCAR homologation test case sled tests with a THOR-50M as validation device were proposed as validation load case (Figure 6). The applicability of THOR in sled tests for validation of a highly reclined position implies certain limitations. In any case the biofidelity of internal ATD measurements in a reclined position is questionable. Thus, the measurement signals of the ATD will be used only as a validation device in comparison to the virtual ATD, but not for the injury assessment, which will be done with the HBM.

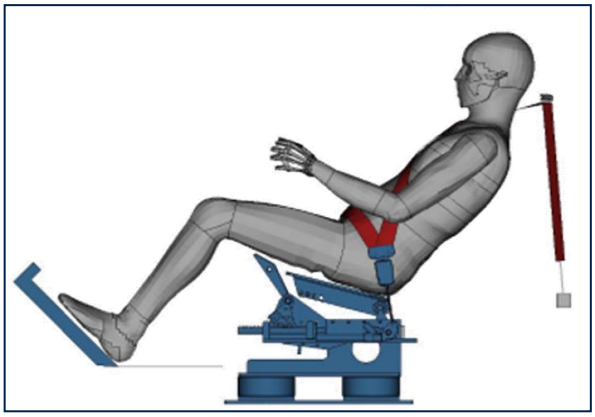

Figure 5 OSCCAR homologation demonstrator

Figure 6 Sled test setup with THOR-50M in reclined seating position (Thorax angle: 48°)

3.1.11 Selection of validation channels

Figure 7 shows a list of channels that were considered suitable and relevant for the validation of the vehicle environment model for HBM-based VT in the OSCCAR homologation test case.

Four repeated tests were conducted that should serve as basis for calibration of the CAE model. To assess the validation status of the calibrated model and certify it for VT one additional test was carried out later. To assess the suitability of a validation channel the CORA value between the mean of the four repeated correlation tests and the certification test and was calculated for each channel. The suitability of each channel was assessed according to the following criterion: $0.8 \cdot Reproducability_{Channel} > 0.58$

One channel (T1 Acc. X) had to be removed as no test data was available. Another six channels T12 FX and FZ as well as all four clavicle forces were removed from the validation procedure as the test scatter was considered too high based on the above suitability criterion.

▪ Restraint System	$F_{B3} - F_{B6} - D_{B1}$
▪ Head C.o.G.)	$AC_X - AC_Y$
▪ Upper Neck	$F_X - F_Z - M_Y$
▪ Thoracic Spine (T1)	~~AC_X~~ $- AC_Y$
▪ Thoracic Spine (T4)	$AC_X - AC_Y$
▪ Lower Thoracic Spine (T12)	$AC_X - AC_Y -$ ~~F_X~~ $-$ ~~F_Z~~ $- M_Y$
▪ Chest Deflection	$UL_{Res} - UR_{Res} - LL_{Res} - LR_{Res}$
▪ Right Clavicle	~~$FX_{,inner}$~~ ~~$FZ_{,inner}$~~ ~~FX_{outer}~~ ~~FZ_{outer}~~
▪ Pelvis	$AC_X - AC_Y - AN_Y -$ Submarining
▪ Iliac	$F_{X,left} - M_{Y,left} - F_{X,right} - M_{Y,right}$
▪ Femur	$F_{Z,left} - F_{Z,right}$

Figure 7 Channels were considered suitable and relevant

3.1.12 Application of the proposed objective acceptance criteria for environment certification

The above-mentioned procedure was applied to simulation results for the OSCCAR validation pilot case and results of one test that was conducted within the OSCCAR project for validation to demonstrate its applicability to Phase 2 of the VT certification procedure (Figure 1).

1) For acceptance, the objective rating has to be above the $OAC_{Channel}$

   21/27 channels (78%) passed the 1st stage certification procedure

2) Channels that do not fulfil this criterion have to be reviewed
   a) Channels with a CORA-value below the $OAC_{Channel}$, but above the threshold of 0.58 might be acceptable. However, justification is necessary:

      4 out of 27 channels failed the acceptance criteria (see Figure 8*), however, the CORA-rating was above the threshold of 0.58. For example, the Upper Neck (Mo. Y) had similar time-history curves, however, deviations in the peak values were observed.*

   b) Channels with a CORA-value below the threshold of 0.58 are not acceptable unless detailed justification is provided:

      Two channels showed a CORA-value below 0.58 (see Figure 8*. The lower right (LR) Chest Deflection was reviewed and decided to be uncritical. For the Left Iliac Moment, the pelvis-to-belt interaction was not predicted correctly, as the position of the belt on the ASIS load cell was different. However, as this issue is a well-known limitation of the simulation model and the submarining was predicted correctly, it was decided that the whole simulation model should not be rejected due to this.*

Channel	Val. Test	Validation Simulation for Certification		
	$OAC_{Channel}$	CORA	CORA > OAC	CORA > 0.58
Upper Neck (Mo. Y)	0.769	0.715	✗	✓
T1 (Acc. Z)	0.639	0.622	✗	✓
T4 (Acc. X)	0.704	0.608	✗	✓
UL Chest Deflection (Displ. Res.)	0.729	0.679	✗	✓
LR Chest Deflection (Displ. Res.)	0.778	0.556	✗	✗
Iliac left (Mo. Y)	0.688	0.298	✗	✗

Figure 8 Channels failing the 1st stage of the objective acceptance criteria

In summary it was decided that the vehicle environment model is sufficiently validated and considered certified for use for VT in Phase 3 within OSCCAR research project applications. However, this decision was taken considering the following limitations that should be addressed before applying this approach in a respective procedure for e.g. consumer testing or even VT-based type approval:

- The THOR ATD was not developed for reclined seating positions. Further investigations regarding the suitability of THOR as appropriate validation device are necessary
- The semi-rigid seat is stiffer in the vertical direction than most production seats resulting in an overestimation of the lower thoracic spine z-forces

- Further improvement of the pelvis-to-belt interaction in simulations are necessary:
    - In the CAE model a new pelvis geometry based on the seated dummy should be used
    - Bending stiffness should be added to belt webbing in LS-DYNA and the corresponding material card should be updated to avoid folding of the belt

- More test data is needed to evaluate and improve method and acceptance criteria

3.2 Standardised naming of reference points in HBMs (LMU, TUG, ZF)

Landmarks are a crucial tool to align and validate simulations with experimental data e.g., from crash test dummies as well as to compare the morphology of HBMs with each other or human participants and post-mortem models. To use similar landmarks in different systems is challenging due to different ways to define those landmarks in virtual models, dummies, or human bodies. Moreover, there is no homogenous naming convention. Therefore, the same landmark might be differently referenced in publication from various groups and harbors the risk of confusion.

This situation constitutes the motivation of the project to find a user-friendly and standardized nomenclature for landmarks. Key features and boundary condition of such a nomenclature are:

- **8 digits length** for compatibility with experimental data loggers
- naming algorithm inspired by **anatomical conventions**
- easy handling for users with a diverse professional background (e.g., engineering, biomechanics, medical science), and
- application of naming codes form **ISO MME Database [4]**

The anatomical naming system applies various technical terms to define orientations and locations at and in the human body. Figure 9 depicts the basic anatomical wording. There are three major planes – frontal, sagittal and transversal – that are defined for the upright standing human being. The extremities due to their high degree of motion have additional wording to clarify orientations.

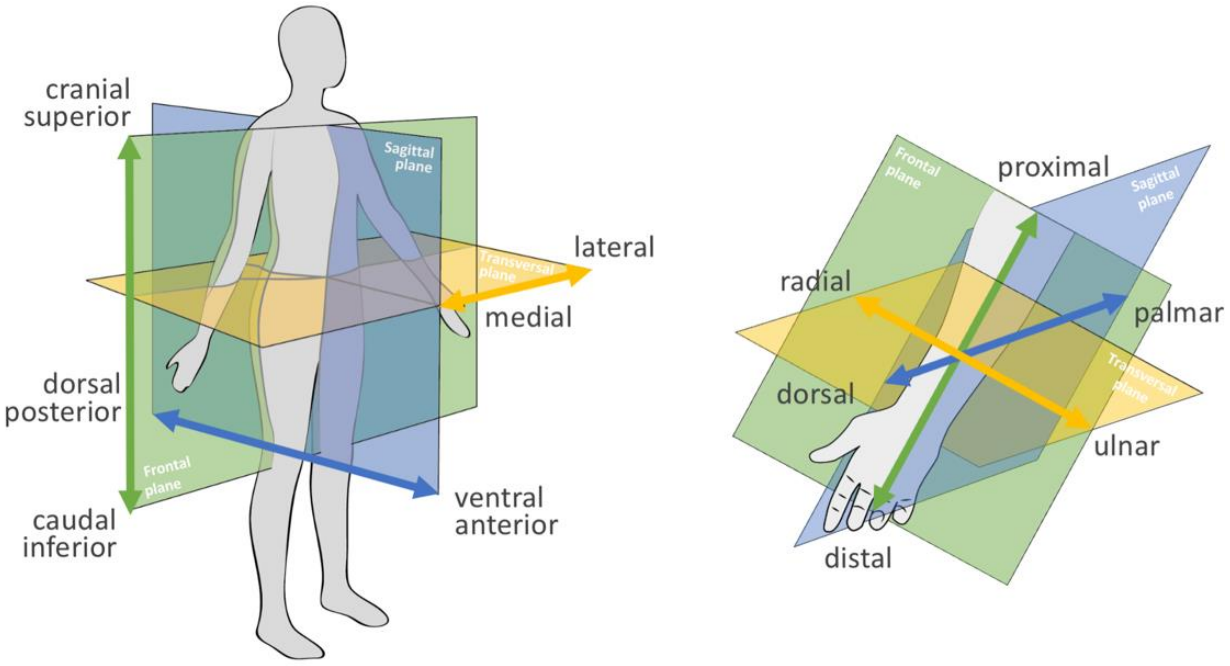

Figure 9 Anatomical orientations and wording

Based on the anatomical naming system and the existing structures for landmark naming in crash test setups by ISO MME Database [4] the proposed naming system consists of:

- a **main location** (4 digits),
- a **global fine location** (1 digit) and
- three **regional fine locations** (each 1 digit).

These locations represent the anatomical coordinate system consisting of a longitudinal axis (in the frontal plane, z-direction), a sagittal axis (in the sagittal plane, x-direction) and a transversal axis (in the transversal plane, y-direction) (Figure 10).

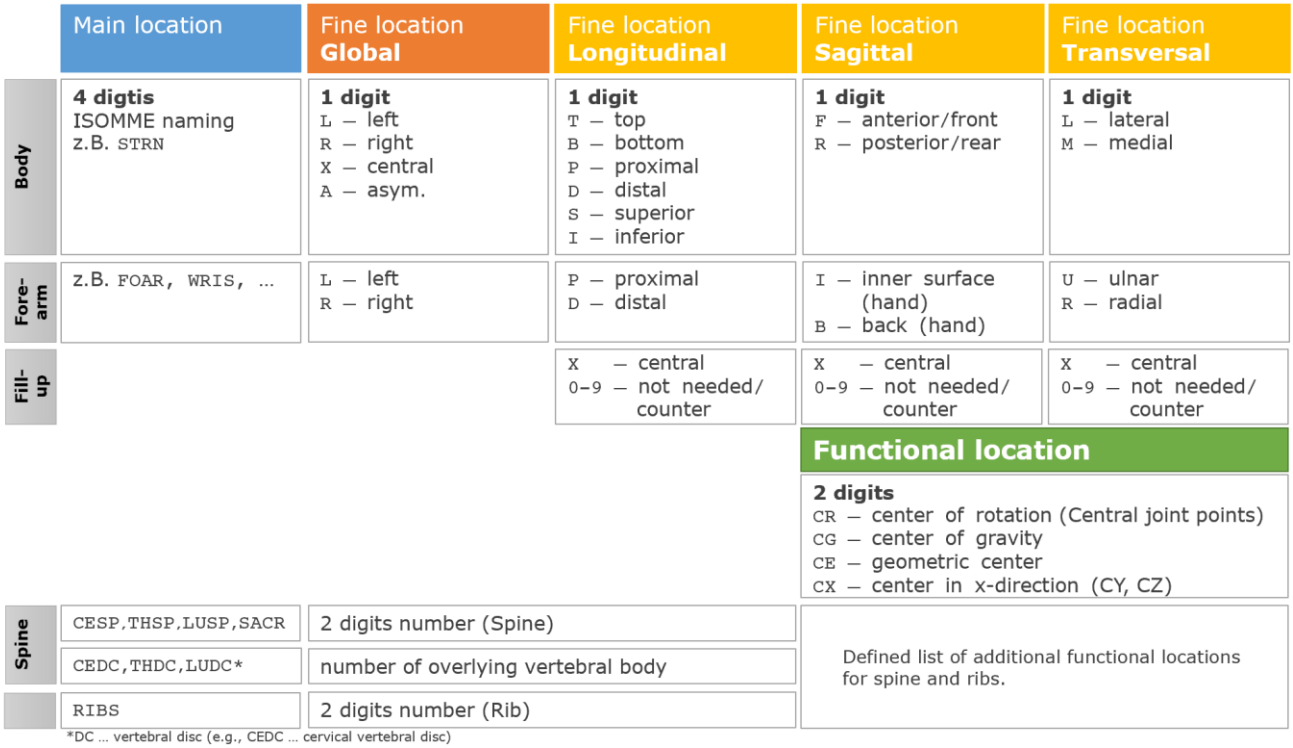

Figure 10 Naming convention

The global location uses standardized names from ISOMME Database e.g., “STRN” for sternum. It defines the global anatomical region. The global fine location specifies the orientation regarding right, left or central. If this naming is not applicable due to the complex structure of e.g. an organ, the location can also be put as asymmetrical. For the fine locations longitudinal, sagittal, and transversal are various naming possibilities to apply for the varied sites of human body structures.

In order to increase the efficiency of the system, a fill-up algorithm within the local fine locations (last three digits) enables the use of numbers and functional locations on the last digits. Functional locations refer to markers like center of gravity, center of rotation, geometric center, or center in x-, y- or z-direction. Functional locations consist of 2 digits names e.g., “CG” for center of gravity and are to be used on the last two digits. If a functional location is used, any local fine location can be placed on the 6th location to fill-up the marker name.

Further, there is the possibility to specify regional fine location with “X” to refer to central positions respectively on the corresponding axis. Therefore, when using this algorithm, all regional fine locations (longitudinal, sagittal, transversal) must be used - there is no fill-up possible to use numbers. For instance, “HEELLXRM” refers to the center of the medial edge of the posterior surface of the left calcaneus.

The fill-up algorithm as well as the correct usage of central positions regarding the regional fine location are illustrated in Figure 11 with marker naming examples.

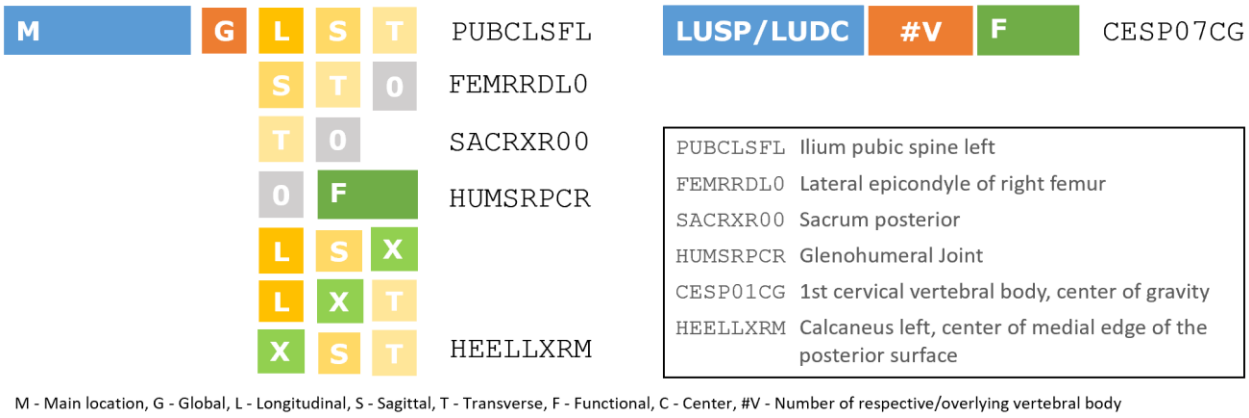

Figure 11 Illustraion of the fill-up algorithm and examples

The body regions forearm, spine and ribcage require exceptional naming. The forearm due to its high degree of freedom is treated equivalently as in the anatomical nomenclature and orients respectively to its back and inner surface of the hand. Therefore, special short naming is used that can be seen in Figure 10.

Additionally the naming algorithm for the spine, consisting of complex structured vertebral bodies and intervertebral bodies, as well as for the ribs uses the 5th and 6th digit for numbering, e.g., 1st vertebral body. Hence, just to digits are left for further specification. A list of functional location is given in Table 1.

In Appendix A (Table 6 to Table 13) a large set reference points, which are relevant for human modelling is shown.

Functional location	Structure	Functional location	Structure
Spine			
TC	Center top plate (vertebral body)	RT/LT	Transverse process right/left
BC	Center bottom plate (vertebral body)	SR/SL	Superior articular process right/left
LC	Left midpoint (vertebral body)	IR/IL	Inferior articular process right/left
RC	Right midpoint (vertebral body)	FR/FL	Transversal foramen right/left
VC	Ventral midpoint (vertebral body)	PL/PR/ PS/PI/ PP	Processus spinosus left/right point, superior/inferior point; furthest posterior point

DC	Dorsal midpoint (vertebral body)	DT	Top Point Dens
TA	Anterior point top plate	DB	Center of Dens basis
TP	Posterior point top plate	AA	Most anterior point Atlas
TL	Left point top plate	AP	Most dorsal point Atlas
TR	Right point top plate	SC	Spinal canal
BA	Anterior point bottom plate	C1/C2	Superior costal facet right/left
BP	Posterior point bottom plate	C3/C4	Inferior costal facet right/left
BL	Left point bottom plate		
BR	Right point bottom plate		
Functional rib locations			
LL/RL	Lateral Point (curvature) left/right	LP/RP	Posterior Extremity left/right
LA/RA	Anterior Extremity left/right		
Functional head locations			
AM	Auditory meatus	OR	Orbitale

Table 1 List of functional locations for the spine, the ribs and the head

3.3 Protocols for harmonised reference point identification (LMU)

In order to get comparable simulation results in VT it is necessary to define harmonised reference points for HBM positioning. These points are needed to establish harmonised pre- and post-processing procedures, to safeguard credible results of HBM simulations and to consequently qulify the models as reliable tools in the safety divisions of automotive companies. For this purpose, in 2018 LMU defined sets of reference points aiming to be used by a broad community of HBM users[5]. The project was conducted within the THUMS User Community [6].

These reference points are defined by using anatomical landmarks in order to calculate joint rotation centers based on anthropometric and biomechanical literature [7–9]. In 2018 reference points had only been defined for upper and lower extremities and thorax. As for alternate driving positions in reclined seating spine angles and head positioning are of special interest, protocols for reference point identification in these body regions have been developed for the OSCCAR project.

Additionally a Matlab-tool, that automatically identifies the acetabulum region and calculates the corresponding hip joint rotation center in an input STL was created in order to provide an user-independent and reproducible method of h-point defnition, that can be applied to a wide range of HBMs.

In this chapter the definitions of harmonized refpoints of the following body parts are described in detail:

- Protocol for the definition of spine reference points including the definition of local coordinate systems for cervical, thoracal and lumbar vertebrae (C1-L12)
- Protocol for the definition of head reference points based on the Franfort plane
- Algorithm for automatically calculating hip joint rotation centers based on STLs

3.3.1 Spine reference points and local coordinate system definition

In order to implement reclined seating positions in different HBMs it is necessary to have local coordinate systems in the vertebrae which define the exact position of a vertebral body and its angle in reference to its adjacent vertebrae. This information is not only crucial in order to ensure comparability between simulation results generated by different users in different models but also between experimental data and finite element models.

The method described here was developed by Draper et al. [10] :

1. Start by identifying both **vertebral endplates** and assigning planes to them. For the finite element model this can be done by finding the best fit plane to all the nodes associated to the endplates. For 3D experimental data, before a best fit plane can be found, the data needs to be segmented, 3D-reconstructed and exported in the form of a nodal structure. The midpoints of these newly created planes are defined as the **center points of the endplates**.

1. Then the best fitting planes associated to the endplates are then averaged in order to generate the midplane. The intersection point between this midplane and the line connecting the two center points of upper and lower endplate defines the **center of the vertebral body (c_{VB})**.

2. Next, in order to define the **local x-axis**, the **centerpoint of the spinal canal** is calculated as interpolated centroid (=arithmetic mean, average position of all points on the object`s surface) based on the selected nodes on the spinal canal ring's inner surface. This center of

the canal ring is then projected to the midplane and named **c_{cr}.** The **local x-axis** is defined by the **line through c_{cr} and c_{vb}.**

3. The **local z-axis** is defined by a normal of the midplane which intersects the **center of the vertebral body (c_{VB})**.
4. The **local y-axis** defined via the cross product of the local x and z axes.

Figure 12 shows the the midplane construction by fitting the plane to the upper and lower endplates and Figure 13 shows the selection of the nodes of the canals ring. Figure 14 shows the definition of the local coordinate axes within the midplane an Figure 15 the final coordinate systems in THUMS 4.2 lumbar vertebrae (L1-L5).

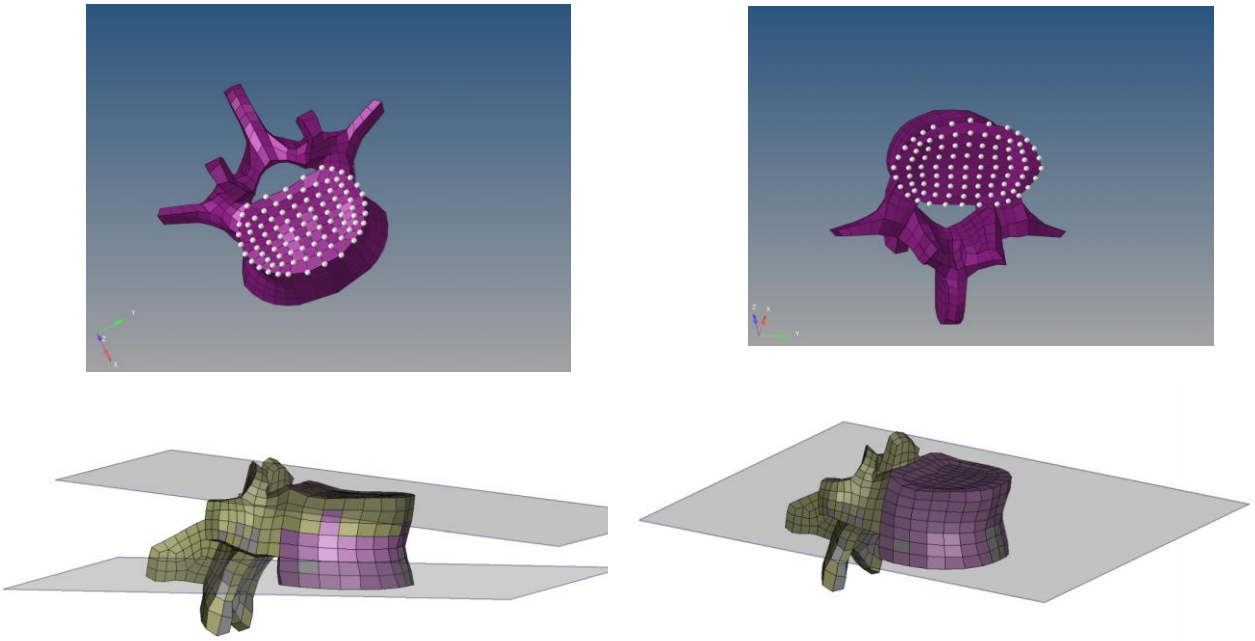

Figure 12 Midplane construction by averaging the planes fitted to the upper and lower vertebral endplates

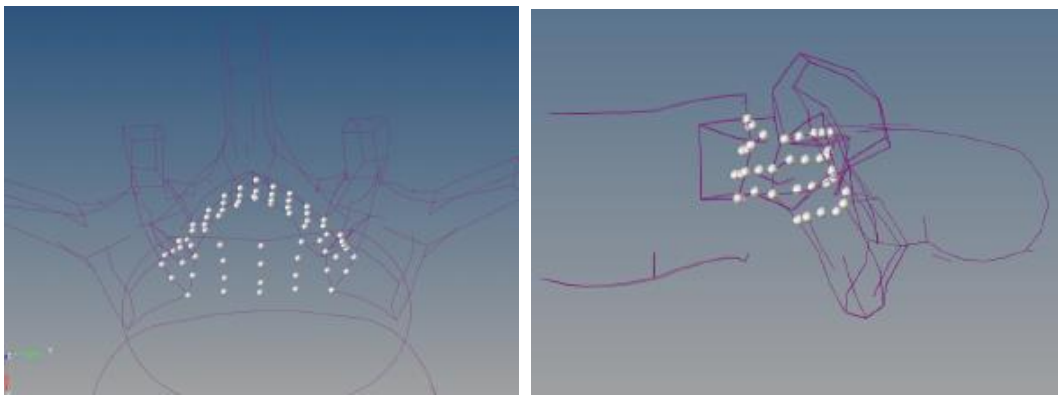

Figure 13 Input nodes for calculation of center of canal ring (c_{cr})

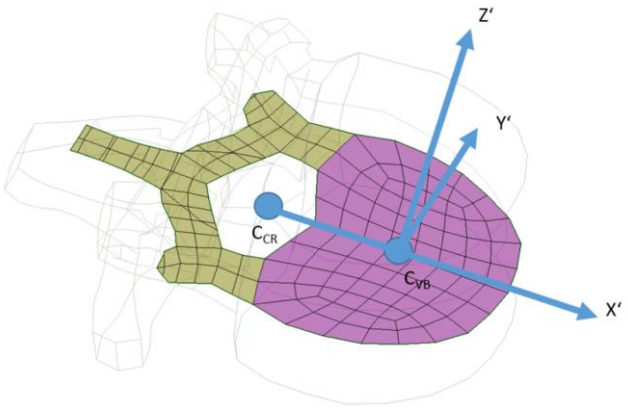

Figure 14 Local coordinate system in midplane with x defined through center points of spinal canal (c_{cr}) and vertebral body (c_{vb})

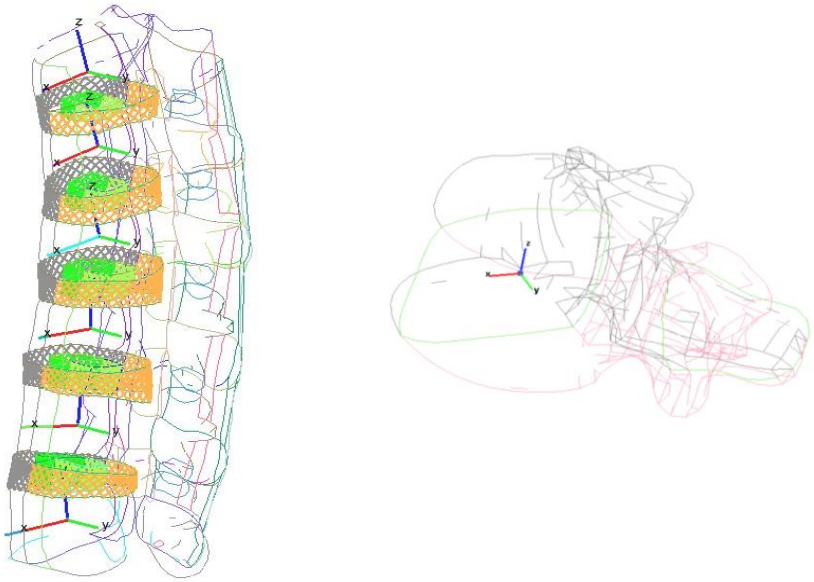

Figure 15 Local spine coordinate system in THUMS 4.2 (L1-L5)

Reference point name	ISOMME ID	Definition
T12 center	THSP12CE	Center and coordinate axes calculated according to Draper [10]
L1 center	LUSP01CE	Center and coordinate axes calculated according to Draper [10]
L2 center	LUSP02CE	Center and coordinate exes calculated according to Draper [10]
L3 center	LUSP03CE	Center and coordinate axes calculated according to Draper [10]
L4 center	LUSP04CE	Center and coordinate axescalculated according to Draper [10]
L5 center	LUSP05CE	Center and coordinate axes calculated according to Draper [10]

Table 2 Spine reference points provided to OSCCAR consortium

3.3.2 Head reference points based on Frankfort plane

In order to make FE simulation results compareable to experimental data, it is crucial to mimic the test subject's position as accurately as possible. As in literature the position of the subject's head is often stated by using the head center of gravity (COG) and the Frankfort horizontal, LMU provided the following head reference points to the OSCCAR consortium for FE models THUMS TUC2020, THUMS V3, THUMS V402 and GHBM (see Table 3).

Reference point name	ISOMME ID	Definition
Head center of Gravity (COG)	HEADX0CG	Center of gravity of the head
External Auditory Meatus (EAM) right	SKULR0AM	Lowest point of external auditory meatus, right
External Auditory Meatus (EAM) left	SKULL0AM	Lowest point of external auditory meatus, left
Orbitale right	SKULLR00R	Middle point of lower orbital rim, right
Orbitale left	SKULL00R	Middle point of lower orbital rim, left

Table 3 head reference points provided to OSCCAR consortium

3.3.3 Script for automatically calculating hip joint rotation centers based on STLs (H-point)

The H-point (or hip-point) is the theoretical, relative location of an occupant`s hip as used in vehicle design, automotive design and vehicle regulation. It represents the pivot point between torso and upper leg portion of the body and is located at the midpoint between the left and the right hip joint rotation centres. As neither the hip joint rotation centres nor the H-point are anatomical landmarks, the H-point needs to be calculated and there are different ways to do that for different use cases (e.g. volunteer testing, ATD positioning, virtual testing…). This can result in different locations of the H-point. In LMUs definition, which was developed in 2018 [6] the h-point is defined as middle point between the left an right rotation centers (see Figure 16 and Table 4).

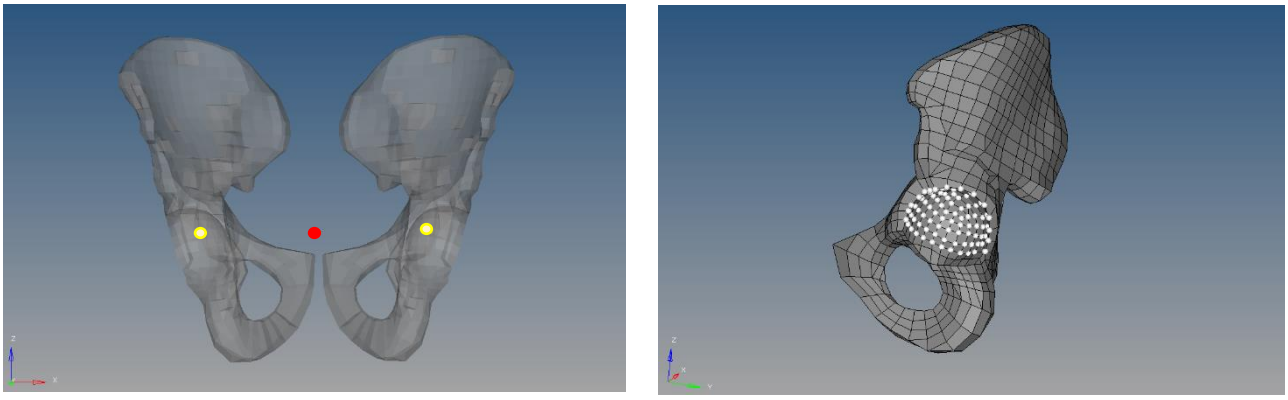

Figure 16 Defining the h-point (red) as midpoint of the hip joint rotation centers (yellow) which are defined as centroids of acetabulum nodes

Reference point name	ISOMME ID	Definition
H-Point	HPNT0000	Midpoint of hip joint rotation centers right and left
Acetabulum right	ACTBR0CR	Hip joint rotation center defined as centroid of acetabulum hemi sphere right
Acetabulum left	ACTBL0CR	Hip joint rotation center defined as centroid of acetabulum hemi sphere left

Table 4 Hip joint reference points

Results of an experiment described in literature can only be reproduced in simulations if the test subject's position is adaped correctly in the HBM. Concerning the definition of hip rotation centers and h- point however there is a wide range of uncertainty which results from different users defining sets of acetabulum points differently. In order to diminish this inter-user discrepancies LMU developed an automated method (Matlab script) which identifies all acetabulum nodes and calculated the acetabulum center (hip joint rotation center) [11]. Figure 17 shows the steps of preparation and data import as well as the steps performed for acetabulum center calculation:

2. First the **area around the acetabulum** is extracted and exported in **STL format**. In FE human models like THUMS or GHBM remeshing the surface in order to get a triangle mesh may be necessary. The STL file, which consists of the tiangles vertices. The **triangles normals** are calculated
3. Then the **slope change** of the associated neighbours of the STL triangles is calculated
4. The ***k-means* clustering algorithm** is applied for clustering the slope-values into two clusters. These clusters are used to identify those triangles, in which the neighboring slope change is very high because they are very likely the ones at the acetabulums rim. As a result the **triangles at the acetabulums border** are detected
5. In the next step a **circle** is approximately placed on these border triangles using the ***Kasa method*** [12] which is basically a least-squares approach. In this method a plane is calculated to which the given points (points of the border triangles) have the smallest distance. Afterwards the given points are projected onto this estimated plane, as the *Kasa* method can only be used for two-dimensional data.

6. After creating the estimated circle, the minimal distances between the **circle normal** and the respective **triangle normals** are found using the algorithm of ***Lumelsky*** [13].
7. Finally, again with the help of the *k-means* algorithm, a **clustering (two clusters) of these distance values** is done to select triangles which can be used for the calculation of the center of rotation of the acetabulum. For this purpose, the coordinates of the vertices of the selected triangles are taken and the point at which the distance-variance to these vertices is lowest is calculated.

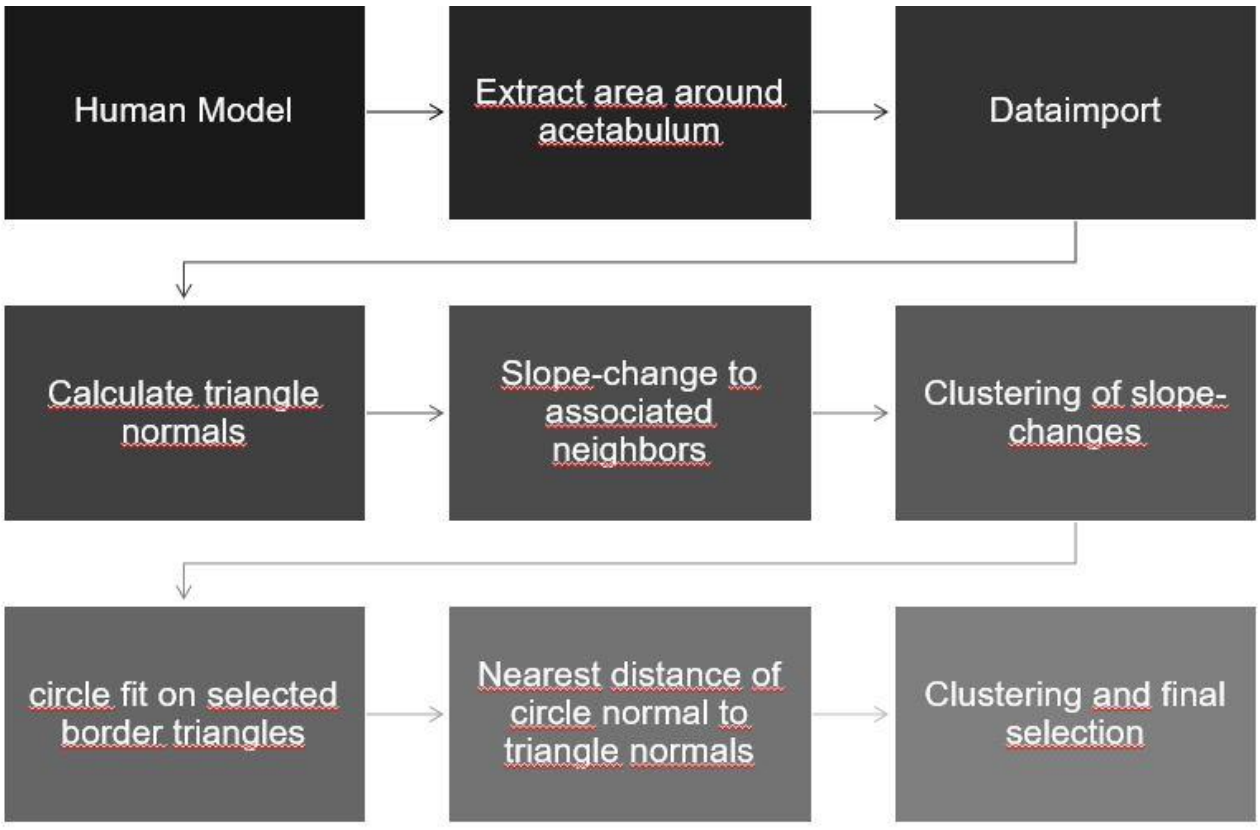

Figure 17 Flowchart of method for automatic calcualtion of hip joint rotation centers based on an input STL of the acetabulum region (method developed by Nikolas Pfeiffer, LMU [11])

The automated script can be applied to acetabulum STLs of remeshed FE models ans those that originated from CT images. Figure 18 shows all steps from STL extraction to final marking of the acetabulum hemisphere at the example of THUMS TUC 2019 acetabulum.

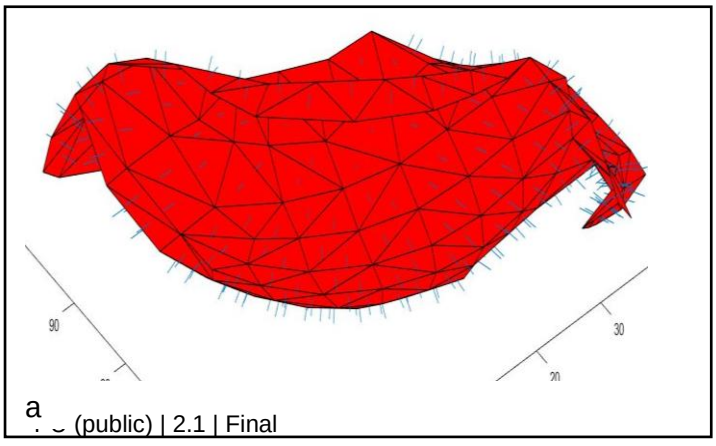

a

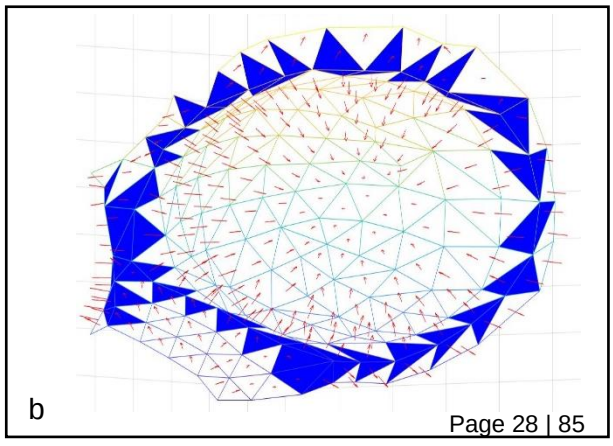

b

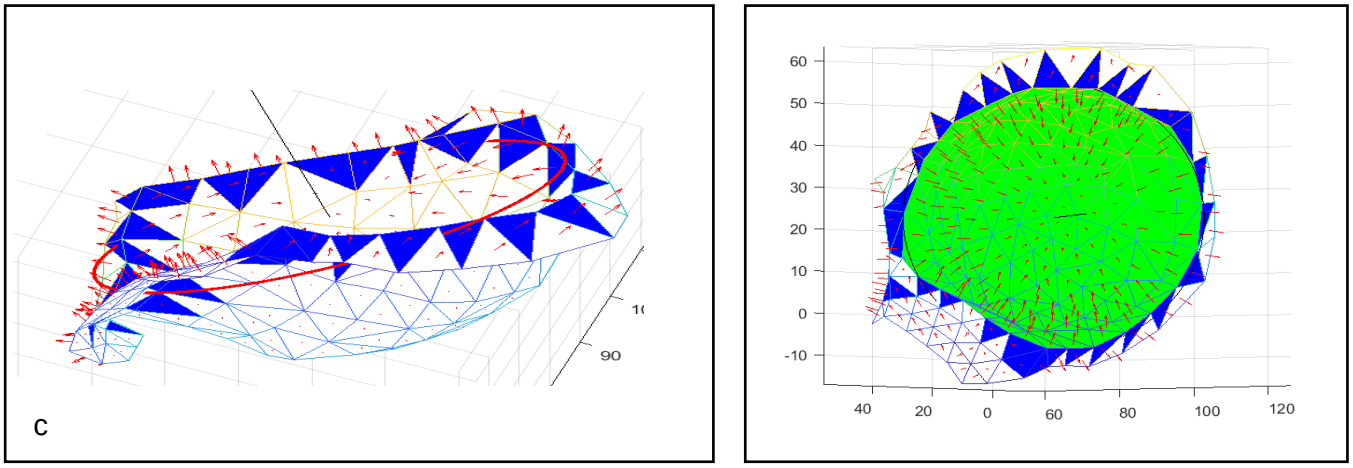

Figure 18 steps of automatic identification of acetabulum border triangles and hip joint rotation center calculation a) imported STL with triangle normal; b) acetabulum border triangles identified by k means algorithm (blue); c) circle fitted with Kasa method (red) and circle normal (black); d) acetabulum triangles for joint rotation center and H-Point calculations

3.4 Volunteer testing protocol (Chalmers, TUG)

HBMs with active muscles are promising tools for assessing vehicle safety systems in crashes when also pre-crash phases are included in analysis of safety systems. For these models to predict occupant motions and restraint systems interaction during the pre-crash phase, they first need to be developed and thereafter validated using data from volunteers. For development of these models, muscle activation levels during the entire pre-crash phase are typically used to identify muscle recruitment patterns. For final tuning and validation of these models, kinematics data are preferred. While occupant kinematics data from naturalistic driving studies may also be used, volunteer tests are typically carried out in more controlled settings and are thus the preferred data type for active HBM developments and validation.

3.4.1 Ethical considerations

The protocol for volunteer tests should be approved by an ethical commission consisting of experts from different disciplines.

The safety of the volunteers needs to be ensured and a *Failure mode and effects analysis* should be performed when planning the tests. When tests are performed in a laboratory, the risk of a testbed failure or emergency braking system failure needs to be minimised to every-day life risks by the use of redundant systems or, better, inherently safe systems. For in-vehicle tests the risk of having a crash needs to be evaluated and minimised. Typically, this requires testing on a test track with no other traffic. In addition, when vehicle installed restraints are modified, or replaced with other restraints, the injury risk must be evaluated in case there is a crash. Whenever new scenarios are tested, an injury risk assessment using Human Body Models should be performed and loads should be compared to real-life data (e.g., rollercoaster).

The storing of volunteer data, especially video data and photos of volunteers, should be described in the test protocol.

Volunteers may be compensated for their efforts, e.g., given cinema tickets or similar. However, compensation must not be at a level which would make participation in a volunteer test attractive only due to the compensation.

3.4.2 Study Design

It is important to consider that the resources are sufficient for the research to be undertaken; sufficient funding and staff. In addition, clear research questions should be phrased and the required statistical power should be determined prior to the tests, i.e. It should be tested that the number of volunteers tested is sufficient for the posted research question.

The study design should be developed together with those that will be using the data. Typically, a research question can focus on muscle activation schemes or kinematics for a given load case. For these research questions a limited number parameters may be sufficient, while those that develop HBMs may need additional data on boundary conditions, initial volunteer posture, etc.

The study design should also reflect how the data will be used in the development of HBMs. For example, laboratory tests are preferred when collecting muscle recruitment data. In such a study, when data will be collected for construction of spatial tuning curves, tests in a laboratory offers several advantages over tests in a vehicle. For this type of test, the loading must be exceptionally repeatable and applied in several directions. However, in-vehicle tests on regular roads are preferred when the most authentic driving or riding situation is required. One example of such a situation would be in tests were the volunteer is driving the vehicle and subjected to autonomous low g-braking. In

these tests, several volunteers would likely try to maintain their head levelled for continues monitoring of surrounding traffic. This test situation calls for test in a regular vehicle on regular roads; a similar laboratory test may not provide data representative of the situation in normal traffic. However, for passengers, monitoring the traffic situation is not important, and a sled environment may be sufficient. Another example would be measurements of head excursion in lane-changes to the right and to the left. When these tests are carried out in a car the responses are possibly not symmetric. This would be due the presence of a side window and B-pillar and the elevated risk of head contact with these structures in one of the directions. However, the responses are likely symmetric in tests without the presence of these structures.

3.4.2.1 Calibration vs. Validation Tests

It is common practice that the muscle strength, muscle activation onset time, muscle co-contraction etc are calibrated in the development of active HBMs. When the model is considered ready, its response should be validated using a unique volunteer data set. Modifications of the tests should be performed, enabling researcher to use some of the study results for calibration and others for validation of their HBM. An example of a slight modification would be the use of a different load case, while an example of a typically modification would be the use of a different loading environment.

3.4.2.2 Volunteer

Volunteers should be selected according to the phrased research question. While most ethical boards require that the test leader presents the load cases it is preferable that the volunteer is not aware of the research question, the timing of the test and not part of the research team.

Risk of injuries during the testing: A prerequisite could be that volunteers have no history of cervical disorders or low back pain.

Volunteers that are recruited for studies of occupant motions and restraint interactions in test that mimics pre-crash vehicle kinematics, should preferably have travelled frequently in the type of vehicle used in the study.

Volunteer anthropometrics should preferably be close to those of the HBM to be evaluated.

3.4.3 Documentation

Anthropometric measures such as the overall height, sitting height, weight, age and sex should be measured as a minimum. In addition, it is advised to measure/record if the volunteer is right- or left-handed, their head circumference, their neck length and their acromion-to-acromion distance.

Questionnaires should be derived supporting the data analysis and explain specific volunteer behaviour based on their well-being during the experiments (e.g., scared, feeling motion-sick, cold, aware of the timing of a particular test, etc).

The initial posture of the volunteer should be documented as well any seat adjustment. These measurements are important when these tests will be replicated in a simulation environment.

Photos of the volunteers should be taken to document the position of all sensors and for analysis of kinetics and kinematics for a given body, e.g., head displacements for head centre of gravity.

3.4.4 Measurements

It should be determined prior to testing how time zero (t0) can be clearly identified from the test data. For proper post-tests data analysis, it is also important that a single trigger signal is use to start all measurements included in the test setup and the following samples are time synchronized.

3.4.4.1 Motion tracking

For proper analysis of volunteer kinematics, tracking points should be selected based on the phrased research question. Head and upper torso linear and angular displacements are usually of high importance. Other kinematics data often used in validation of HBMs are shoulder and hip displacements. Sensitivity studies have shown arm position to significantly influence head and torso responses in pre-crash manoeuvres and tracking points on the arms should also be included.

Cameras and lenses should be calibrated prior to each test series, or ideally each day to make sure that the captured data is useful in the final analysis. Typically lens calibration is only required when lenses have been shifted or focal length have been modified (for zoom lenses). Recordings of reference targets, used to define joint coordinate systems for all used cameras, may have to be captured frequently. Frequency is a function of the sturdiness of camera mounts and if camera position has to be changed between test series.

The location of the tracking points should be clearly documented (pictures + description how they were picked). The initial location of the tracking points at t0, for each individual or for the mean person, should be evaluated and published together with the test data.

3.4.4.2 Boundary conditions

Preferably all boundary conditions should be recorded if data are to be used for HBM evaluations. Boundary conditions for seated volunteer in the passenger seat would likely be foot forces, any interaction forces between vehicle interior and arms, seat cushion and seat back deformations, belt forces and belt pay in/out.

Belt forces should be measured at comparable locations for each volunteer. In addition, belt geometry should be documented.

In laboratory tests, measurements (e.g., forces on the seat cushion) can be performed more easily than in a car.

Pressure distributions between a volunteer and seat cushion or seat back can be recorded with a pressure mattress or mattresses. When using these mattresses, it is important to record their location relative to the volunteer/seat surfaces and mattresses should be calibrated.

Any effect of inertia of supports/seats etc on measured load cell signals should be evaluated by pursuing complete set of tests without the volunteer in the set up.

3.4.4.3 Muscle activity

When measuring muscle activation with electro myography (EMG), the data should be normalised by each muscle's isometric maximum voluntary contraction (MVC) that is collected in separate tests. EMG data and MVC signals should be processed ideally directly after tests, or signal quality monitored in-between tests, to make sure that all sensors work properly. The analyses may reveal loose sensors, pressure artefacts, or that EMG signals are reduced.

3.4.5 Data analysis

A common way to present volunteer response data is to calculate average values and standard deviations for each time step and plot these as a function of time. When constructing these response corridors, it is important that these corridors are compared with individual responses. If an average response is not representative of the shape of the bulk of the volunteer responses, for a given parameter, then additional analysis should be carried out. An alternative or complementary method to present the result are to present parameterised measurements (onset time, peak time, peak). These could be used to establish a generic response curve or for more advanced data analysis.

3.5 Code-specific requirements for pre-processing and post-processing (ESI)

3.5.1 Introduction

The objective for defining code-specific requirements is to ensure compatibility between crash codes.

- To enable an easy comparison between model definitions and simulation results
- To minimize the source for error when translating from one code to another
- To minimize the deviation in simulation results due to implementation of different algorithms

A basic requirement is that models from different codes should share the same topology, with the same number of FE entities, same identifiers and same nodal coordinates.

Objectives:

- Compatibility between different crash codes to ensure that all final results are code independent
- Crash code independent harmonization of simulation settings (e.g. control settings etc.) between different models that will be combined in a VT procedure e.g. vehicle model and occupant model. Compatibility needs to be ensured in validation load case simulation as well as in homologation or assessment simulation
- Definition of code-specific quality requirements for pre-processing (numerical correctness, discretization, convergence, element quality, control settings etc.) and code-specific requirements for post-processing: (energetic balances, added mass percentages, hourglassing, damping) as input for WP4 (for virtual vehicle environment)

Furthermore, as many options as possible should be harmonized. With different options available a strong focus should be put upon compatible options. Incompatible options should not be used in the favor of alternative modelling.

Options with known influence on compatibility are

- Control settings such as time step control or element control
- Numerical implementation of different algorithms for contact or element formulations
- Solver versions and precision

3.5.2 Code specific requirements for pre-processing

The code specific requirements for pre-processing can be subdivided into the following topics.

3.5.2.1 Simulation time step control

Prior to running the simulation, a data-check simulation should be performed to preliminarily check and confirm the time step after initialization as well as the initially added mass resulting from time step control.

The initial timestep should be “code independent” for the whole virtual testing and validation process and consistent between different models to be combined within the process, e.g. vehicle environment and occupant. Furthermore the actual solution timestep in the solver output listing should correspond to the target time step defined in the time step control blocks.

The initially added mass resulting from the timestep control should be orders of magnitudes lower than the total mass so that its influence can be neglected.

3.5.2.2 Control parameters definition, local versus global level

The influence of globally defined control options must be checked. Ideally options defined on local card level are not overwritten by global definitions. This way a change of the global control header after distribution of models does not influence the results. In case that global definitions overwrite local definitions, unconventional or not widely used settings should be avoided again with focus on common options between codes.

3.5.2.3 Output parameters

Output settings such as contour and time history interval should be code independent and harmonized for the whole process to enable easy comparison of results.

3.5.2.4 Contact interfaces

Differences in implementation of contact algorithms need to be considered, such as

- penetration treatment (depth, min. remaining contact thickness)
- contact stiffness
- friction coefficient (static, dynamic)
- entities with friction treatment (nodes, segments, edges)

The model should be checked for initial penetrations. In case these result from a pre-simulation they may be considered noncritical. Otherwise the initial penetrations should be removed either by modifying the coordinates of the respective nodes or by modifying the contact parameters. For stability reasons care should be taken to then assure enough minimum remaining contact thickness in both codes.

Influence of initial penetrations on the initial time step of the model need to be assessed. In this context parameters for non-linear contact stiffness in VPS should be avoided – otherwise they may lead to a reduced initial time step together with the active nodal time step scheme.

In case of instable contacts, one should first try to increase the active contact thickness before increasing the contact stiffness due to the possible influence on model time step.

The VPS solver does not differentiate between static and dynamic friction coefficients, whereas the LS Dyna solver does. In the load cases investigated it has proven to be acceptable to degenerate the more complex friction model from LS Dyna to match the simpler friction model of VPS.

The formula for contact friction coefficient from the LS Dyna manual is

$$\mu_c = FD + (FS - FD)e^{DC|v_{rel}|}$$

with FD/ FS : dynamic/static coefficient of friction, DC: exponential decay coefficient and v_{rel} : relative velocity of the contact surfaces. Setting the exponential decay coefficient $DC = 0$ gives

$$\mu_c = FS$$

which represents friction coefficient behavior as from the VPS solver.

Another difference in results may originate from edge entities for which friction behavior may not be implemented. This has proven to play a significant role when coarsely meshed and highly deformable parts interact through contact.

In order to understand differences and improve the edge contact behavior a rope friction test case with a known analytical solution has been generated.

In the test case from Figure 1Figure 19 a 2d belt model of 50 mm width is wrapped around a rigid cylinder with 300 mm diameter. Mesh size and contact definition corresponds to the HBM model test case. At one end an axial force of 2 kN is applied and kept constant, the other belt end is loaded with a prescribed motion to reach a longitudinal displacement of 450 millimeter after 100 milliseconds, see also Figure 20.

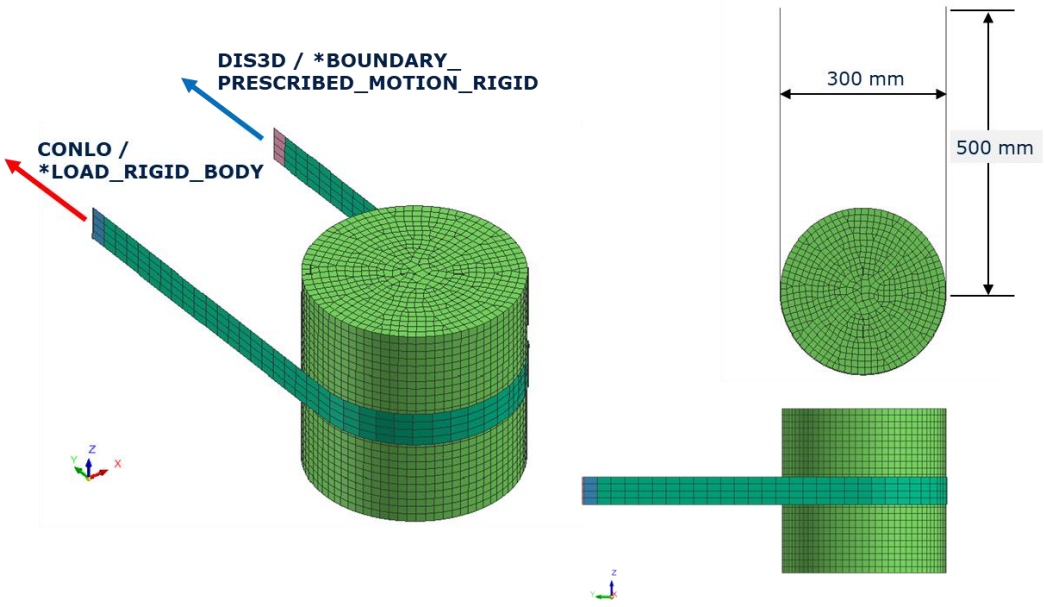

Figure 19 Rope friction test case for comparison of edge friction behavior between LS Dyna and VPS

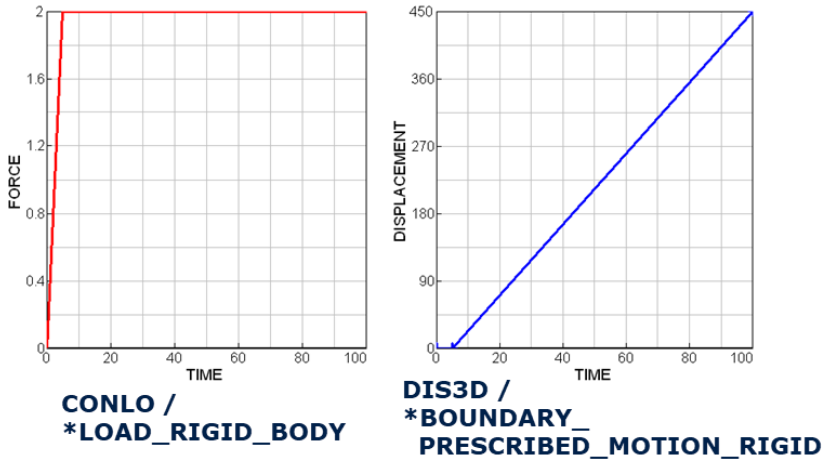

Figure 20 Curves for force and displacement loading at belt ends

Displacements at both belt ends are evaluated as well as the belt reaction force at the belt end with kinematic loading. The analytical solution for increased belt force F_1 due to belt/rope friction can be written as follows

$$F_1 = F_2 * e^{\beta\mu}$$

with F_1: increased belt force due to contact friction, F_2: lower belt force, β: belt opening angle in rad (see also Figure 21 and VPS user's manual, belt slip ring definition, usage and rules, slipping condition).

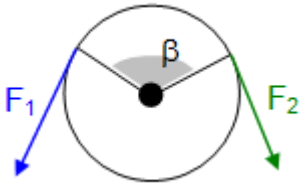

Figure 21 Belt routing, belt forces F_1, F_2 and opening angle β

With a lower belt force $F_2 = 2kN$, an opening angle $\beta = \pi$ and a friction coefficient $\mu = 0.5$ the target belt force computes to $F_1 = 9.6\ kN$.

The following setups with respect to cylinder mesh size and mesh warpage angle have been assessed

- mesh size 25 mm (as in hbm load case), warpage angle 3.5 degrees
- mesh size 12 mm, warpage angle 0. degrees

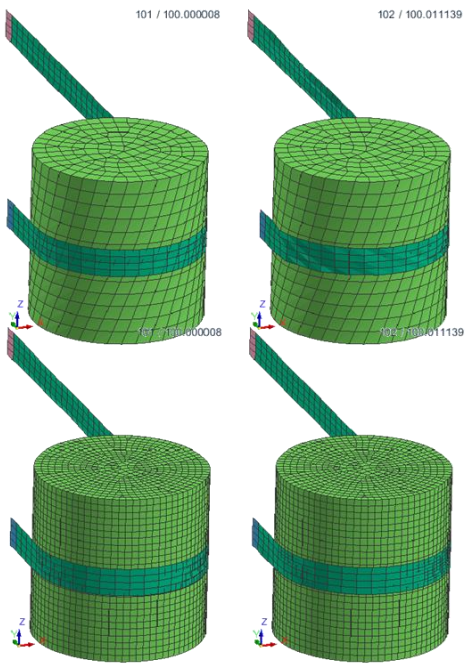

Figure 22 coarse and warped versus fine and even cylinder mesh (left: VPS, right: LS Dyna)

Figure 23 show displacements as well as forces at both belt ends for the configuration with coarse and warped cylinder mesh. The black line denotes the target force computed from the analytical formula. It can be observed that the maximum belt force in the LS Dyna simulation stays significantly below the target. The force in the VPS simulation stays close to the target but oscillates due to belt slippage.

When changing the cylinder to a more fine and even mesh without any warpage the results in both codes align close to the target belt force, see Figure 24.

Consequently, large contact areas with warped element surfaces should be avoided and the mesh of both belt and HBM in the region of interaction refined to avoid friction loss effects. The maximum allowed mesh size depends on the model and the load cases and may have to be re-evaluated in the course of the process. Ideally it should be assessed with representative component tests prior to a series of investigations to avoid repetetive work. Adding some (realistic) bending stiffness should also help avoid excessive element warpage and friction loss through edge contact.

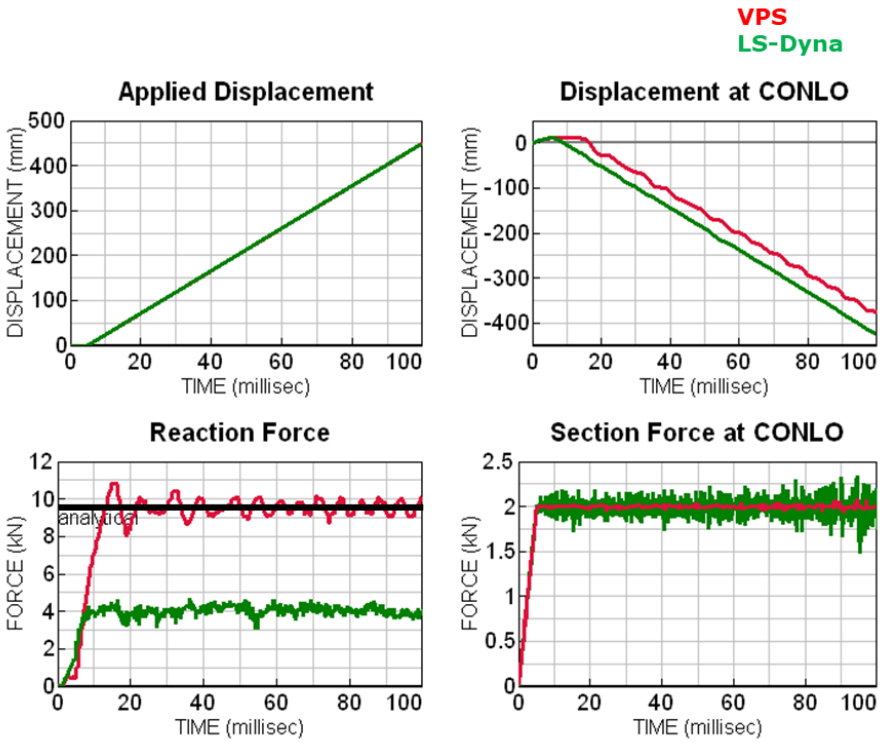

Figure 23 Loss of friction force in LS Dyna with coarse and warped cylinder mesh

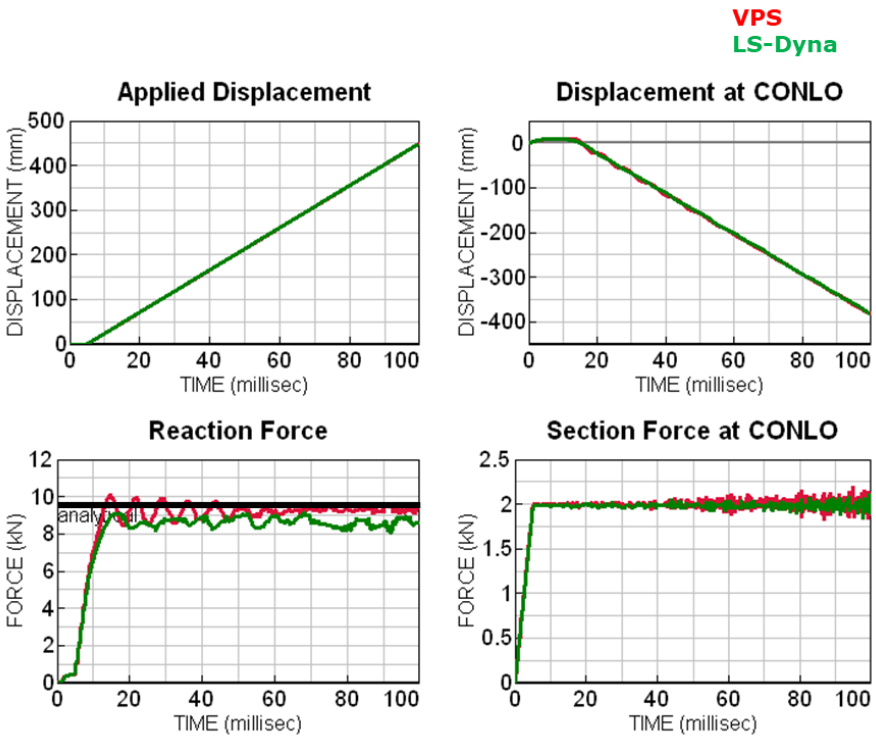

Figure 24 Improved belt force in LS Dyna for a fine and even cylinder mesh

3.5.3 Element formulations and element mesh

Element formulation for 1D/2D and 3D entities should be chosen considering aspects of

- Stability
- Robustness
- Realistic results compared to experiments
- Compatibility between codes

Under-integrated elements can be chosen to reduce the computational efforts. While doing so some numerical aspects have to be considered.

- Appropriate hourglass control and viscosity parameters should be assigned depending on material properties. For VPS the ESI Input Checker tool can be utilized to check for recommended combinations of material type, hourglass control and viscosity parameters.
- For 3D solid parts the number of through thickness elements should be noticeably higher than just one element, otherwise the bending stiffness of this region is considered insufficient. In this case it is recommended to utilize fully integrated element formulations.

Fully integrated elements can be chosen when hourglass prevention or bending stiffness of a part is assumed to be insufficient. The computational cost of a model should be monitored.

The model mesh should be chosen such that mesh quality criteria in all codes are met. A possible difference in computing the element time step for the different codes needs to be anticipated and checked in each code with similar material definitions assigned.

Also, very large internal element angles close to 180 degrees lead to a solver error at initialization for VPS and should be avoided.

Possible mesh improvements required by one code should be adopted by models for each code in order to minimize differences in results and assure maintainability of the models.

3.5.3.1 Material definitions

The translation of material models between LS-DYNA and VPS requires special attention. There are simple models which can be translated directly without any issue while there are complex models which cannot be translated directly and consequently need to be fitted as best as possible.

In or-der to evaluate the results of different material models in both codes, proper single element testing procedures with various loading conditions are recommended i.e. tensile, compressive and shear testing. The latter should be performed for simple and shear loading.

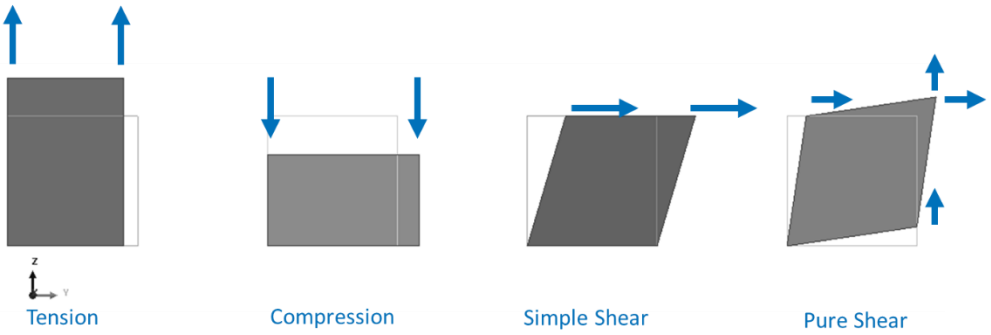

Figure 25 Single element test cases for material calibration

In addition, the applied load should be smooth and displacement driven and the procedure should be repeated for different loading velocities, element types and numerical settings (i.e. hourglass controls, integration rule) to fully cover the complete range of application. For evaluation purposes stress vs. strain or stress vs. time can be considered. In terms of prescribed motion by displacements and the evaluation of engineering stresses and strains both evaluation procedures will show the same characteristics.

In the following, two examples for the translation of material models from LS-DYNA to VPS will be considered. A simple pure elastic material connected to a shell element and a more complex foam material for solid elements. Both materials are taken from the Generic Interior Model and represent the seat cover and the seat foam, respectively.

```
*MAT_ELASTIC_TITLE
$#                                                                  TITLE
MATL9_7608251.1
$#     MID        RO         E        PR        DA        DB
   7000005    1.5E-6     0.015      0.45        0.        0.
```

Figure 26 Example *MAT_ELASTIC, shell element (UI)

As visible in the LS-DYNA material card above the material properties are simply defined by density, Young's Modulus and Poisson's Ratio. Consequently, this kind of materials can be easily translated by automated tools (i.e. Converter in Visual Crash Pam). However, each converted material should be verified by the single element test procedure described before.

The corresponding results in terms of stress vs. time relation of the material are represented in the diagrams of Figure 27. Here the upper part shows the behaviour for both explicit finite element codes for tension and compression, respectively. The lower diagrams illustrate the response under shear loading. It is obvious that for this kind of materials no differences are visible.

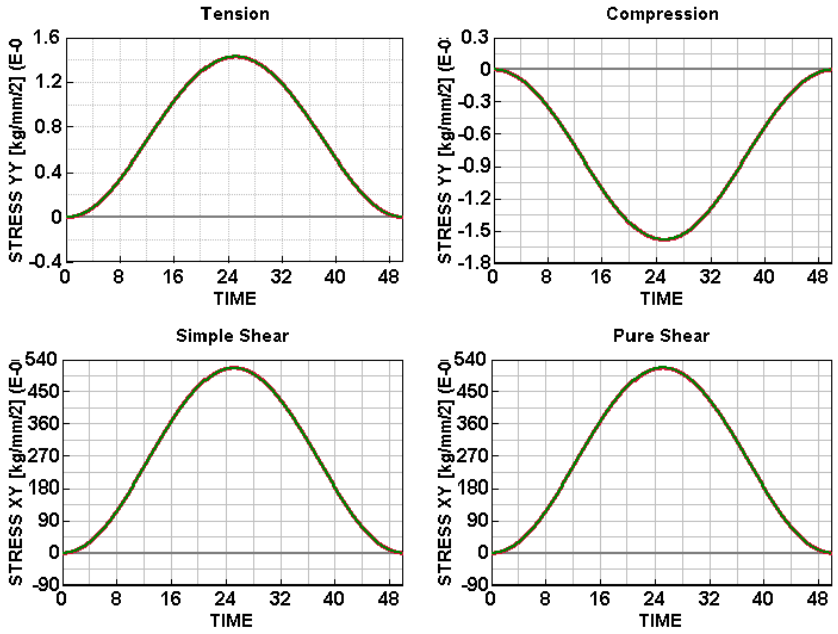

Figure 27 Comparison results LS-DYNA (green) vs. VPS (red) for single element testing for pure elastic material represented by SHELL elements

```
*MAT_LOW_DENSITY_FOAM_TITLE
$#                                                                  TITLE
Bolster OM4IS Foam
$#     MID        RO         E       LCID         TC         HU       BETA       DAMP
   7000013   1.01E-7   0.00416    7000006         0.       0.01         0.       0.05
$#   SHAPE       FAIL     BVFLAG         ED      BETA1       KCON        REF
      10.          0.         0.         0.         0.         0.         0.
```

Figure 28 Example *MAT_LOW_DENSITY_FOAM, solid element (SRI)

Considering a more complex material, like the **MAT_LOW_DENSITY_FOAM,* shows that in some cases a direct translation of the individual settings is not possible. Here, the existing LS-DYNA parameters HU, BETA and SHAPE, describing the unloading behaviour of the foam material are not available in VPS.

Consequently, the unloading behaviour and the related energy absorption of such a material needs to be calibrated with existing options by engineering work. The results of this work for the seat foam material card of the Generic Interior Model shown above are depicted in the diagrams of Figure 29. In correspondence to the previous section, four different element test cases are considered. Analysing all load cases show an almost identical loading phase in both finite element codes, however differences in the subsequent unloading phase which is related to non-compatible options in LS-DYNA and VPS. In order to overcome the issue, a best fit based on the occurring energy absorption in LS-DYNA, has been done with existing options in VPS.

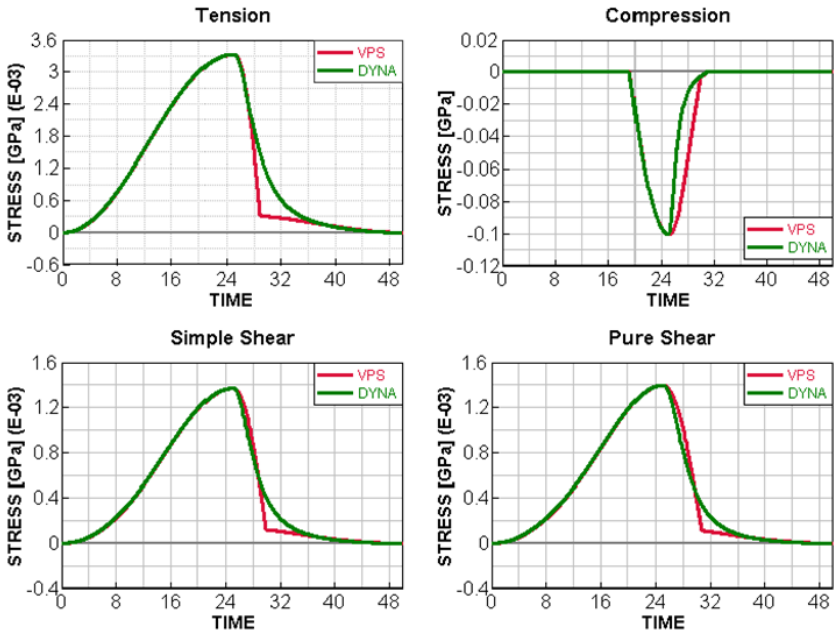

Figure 29 Comparison results LS-DYNA (green) vs. VPS (red) for single element testing for foam material represented by SOLID elements

The described procedure reveals that the strong differences in the effort of material model translation can occur and it might happen that some material models are not compatible between both finite element codes. In these cases, the general range of application should be carefully reviewed to decide which options or features might be negligible.

In similar ways, special options or non-compatible options between the two codes out of the scope of materials needs to be treated. Here, the challenge and time-consuming part is the generation of proper test and validation cases.

3.5.3.2 Solver start parameters

Results should not be significantly influenced by a variation of start parameters such as

- Shared- or distributed-memory processing mode (SMP / DMP)
- Single or double solver precision
- Number of CPU cores and domains in DMP mode

In case significant scatter is observed the root cause in the modelling should be identified and at best an alternative found.

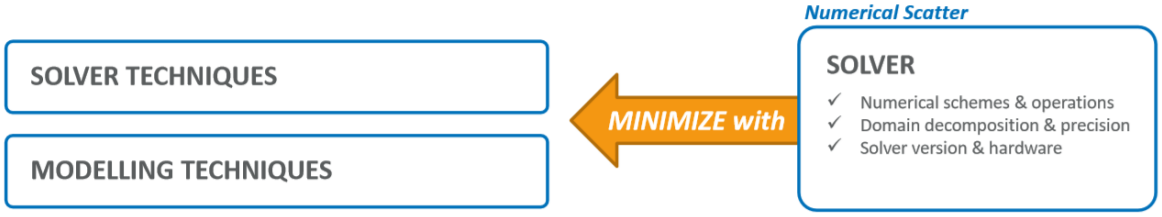

Figure 30 Scheme to minimize unphysical numerical scatter

Unfavorable modelling with respect to numerical scattering can be e.g. crossing material curves or material curves with zero slope. In these cases the response from the solver for specific loading conditions is undetermined. Scattering and even stability issues are likely to occur.

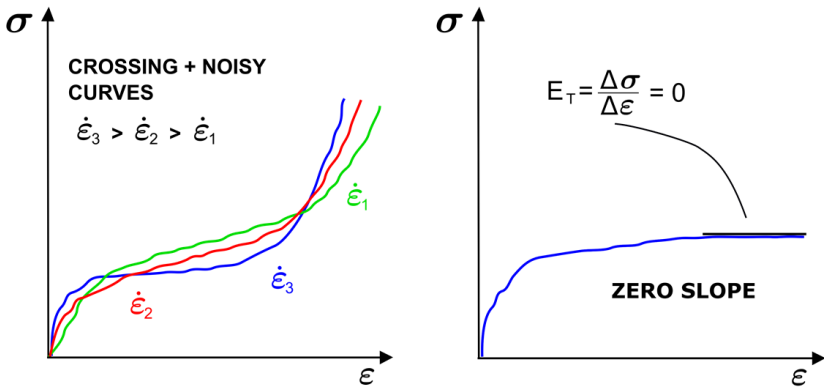

Figure 31 Example for unfavorable definition of material curves with respect to numerical scattering

3.5.4 Code specific requirements for post-processing

To avoid complicating comparison of results between codes the following output control settings should be aligned:

- the time interval for contour output
- the variables for contour output, such as stress/strain measures

Certain numerical quantities should be evaluated for every simulation independent of the code in order to check the simulation for plausibility:

- Global energies
  - Total energy
  - Internal energy
  - Kinetic energy
  - Hourglass energy
- Eternal work, damping work
- Added mass total and per part
- Stable time step

The following plot gives examples for the global energies. While total energy may deviate between codes depending on different energy types considered the global kinetic and global internal energies should be comparable between codes.

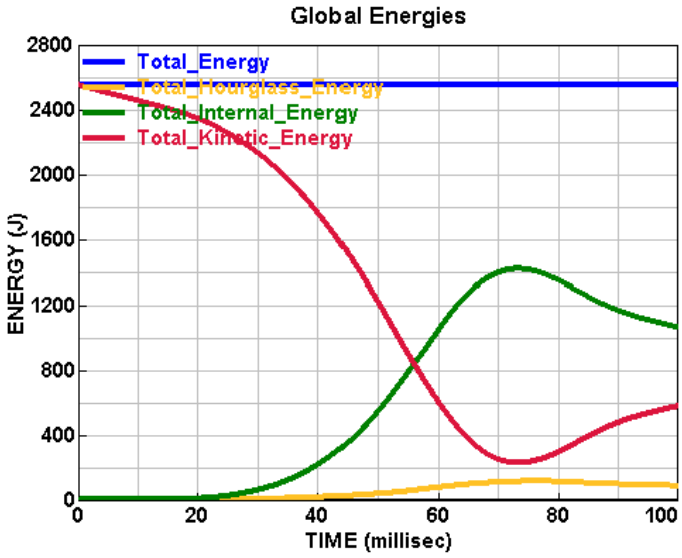

Figure 32 Global energy plot example

3.6 Public load case modelling reclined frontal impact (Autoliv, BASt, ESI, LMU, Siemens)

HBMs need further attendance in terms of validation for new seating positions associated to automated driving. The first available set of data in this context of full-scale experiments has been addressed in OSCCAR. Modelling of those experiments has been addressed with the objective of providing publicly available simulation elements.

3.6.1 Semi-rigid seat

The semi-rigid seat used within OSCCAR was initially developed and used by [14] to assess the submarining behaviour of PMHS in an upright seating position. Furthermore, the seat was used by [15] in combination with protection principle 3 from OSCCAR Task 2.3 (State of the Art belt with Double Lap belt Pre-Tensioning) to define biofidelity targets and describe the biomechanical response of PMHS in reclined seating positions. Besides these two test series, the semi-rigid seat is currently used in a PMHS test series conducted by University of Michigan Transportation Research Institute (UMTRI) and Medical College of Wisconsin (MCW) and will be used in the ENOP project.

Unlike generic rigid seats used in previous test series (e.g. [16], [17]), the seat pan and anti-submarining ramp are pivoted, hence better replicating the behaviour of production seats. Thereby, the rotary movement of the seat pan is counteracted by three springs (two on the side; one in the centre, which is loaded after approx. 8° of rotation), while the rotational motion of the anti-submarining ramp is transformed into linear motion via rack and pinion, here, the stiffness is characterised by two horizontal springs. The stiffness of the seat can be modified by changing the springs (front / rear seat set-up).

Table 5 compares the different mechanical designs and specifications of the semi-rigid seat as used in the different projects. In order to avoid contact between the seat pan and anti-submarining ramp the seat pan was shortend by 20 mm for the PMHS tests at UVa. Furthermore, springs with a slightly different stiffness were used. For the ENOP project the mechanical design has been revised. By that, the rebound of the springs will be prevented by three dampers (one damper for the seat pan and two dampers for the anti-submarining ramp). In order to provide enough space for the seat pan damper, the central spring of the seat pan was moved to a different position while the stiffness was

adjusted accordingly. However, all versions of the semi-rigid seat should have a comparable stiffness.

Feature	Sub-BIO	UVa	ENOP
Seat Pan Length	300 mm	280 mm	280 mm
Springs Seat Pan Side (SS)	127 N/mm (2x)	128 N/mm (2x)	128 N/mm (2x)
Springs Seat Pan Center (CS)	365 N/mm (1x)	379 N/mm (1x)	350 N/mm (2x)
Engagement Center Spring	8 deg / 28 mm	8 deg / 28 mm	t.b.d.
Rebound Seat Pan	Yes (Mechanical)	Yes (Mechanical)	Yes (Damper)
Seat Pan & Load Cell Configuration	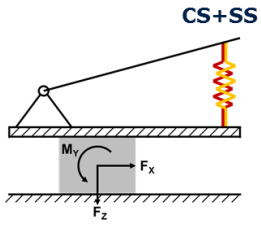	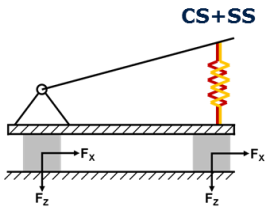	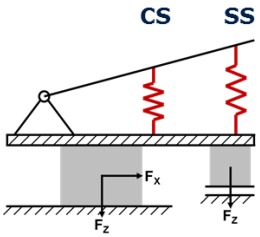
Springs Anti-Sub Ramp	123 N/mm (2)	132 N/mm (2)	132 N/mm (2)
Rebound Anti-Sub Ramp	Yes (Mechanical)	Yes (Mechanical)	Yes (Damper)
Stop Anti-Sub Ramp	No	No	t.b.d.
Load Cells	1	3	2

Table 5 Mechanical design and specifications of the semi-rigid seat as used in different projects

For future assessment of the validity of HBMs in reclined seating positions, a model of the seat used by [15] has been published on the TUC website in VPS and LSDyna crash codes. In addition, the seat model is also available in Madymo between these two codes on the OSCCAR-internal webpage. The code-specific requirements described in this report have been considered for this multi-code modelling.

3.6.2 Belt and Retractor

The belt deserves increasing attention in modelling concerning load cases potentially leading to critical belt interaction and slip-off. One of the major challenges there is the uncontrolled folding of the belt around its longitudinal axis. Two aspects are particularly relevant for such phenomena: the bending stiffness of the webbing and the modelling of the slip rings.

One-dimensional modelling of the slip rings allows easy rotation around the longitudinal axis on that ring. It was therefore recommended to use as minimum 2 one-dimensional slip rings, one at each lateral end of the belt not allowing lateral movement of both rings in the used crash codes LSDyna, VPS and Madymo. A modelling including a fully meshed belt and according contact would be in line with this requirement.

The belt webbing can potentially introduce uncertainties or incorrect responses if causing unrealistic folding and thereby influencing the belt-to-occupant contacts. An approach to increase the bending stiffness by introducing one-dimensional elements in each belt membrane element was reviewed. Finally, the approach proposed by TUC was rated to be appropriate for such load cases. This

approach adds an additional shell layer to the membranes in order to be able to mimic a higher bending resistance, which can be assessed through a so-called omega test or similar. The overall stiffness in tension then needs to be adjusted thereafter, to compensate the additional shells.

Several approaches to model retractors were discussed. A first approach is the modelling by a restraint systems developer and sharing in an encrypted format. This way, the internal knowledge can be easily used but translations to other crash codes either need to be done internally or they can only be done as indirect calibration to the existing encrypted model. Further modifications on the retractor would involve complex procedures and high efforts. This approach has been used in the earlier activities in WPs 2 and 4, but was seen to be of limited applicability for long-term validation purposes.

Another option discussed was the application of generic retractors developed in the context of farside-validation load case modelling by Autoliv and TUC. That retractor has been modelled in two crash codes and made available to the public. For the specific needs of the frontal reclined-occupant loadcase, it was seen to be advantageous to address those needs with a completely new model.

Autoliv, in cooperation with SAFE-UP project, have set up a retractor model that can be fully parametrised to depict pre-tensioning and force limiter and can be implemented on the three anchorage points. It is advisable to use such model as generic representation as future testing in related set-ups will likely involve more advanced restraint options.

3.6.3 Interaction between Belt and HBM, contact algorithms and mesh size

In the course of the project it was found that contact algorithms between highly deformable HBMs and belt systems can bear the risk of friction loss in combination with edge treatment, especially when coarsly meshed surfaces undergo large deformations. If the portion of heavily warped segments from the total number of active contact segments becomes too large the user may have to increase the friction coefficient artificially for improved correlation to experiments.

In combination with different implementations of contact algorithms in the various codes this may lead to inconsistent friction coefficients or results.

Simulation results with HBMs and belt systems should always be checked for this effect. One proven countermeasure would be a local mesh refinement of the belt and possibly also the HBM.

3.6.4 Experimental targets

In PMHS experiments in occupant setups, it needs to be decided how the D-ring position is adjusted for the individual. In the experiments addressed here, it was attempted to keep the belt angle (leaving the shoulder region) constant, resulting in individual D-ring positions. Those are suggested to be averaged as simulation input. An alternative approach would be averaging the actual angles as a single representation in ths simulation.

For the future, it is seen as appropriate approach to average the positioning data from included PMHS as well as the kinematic corridor data, including the measurements of the direct occupant environment.

An important point to be further discussed in this context is the way of positioning the belt (apart from the D-ring position) in non-individualised HBM simulations for validation purpose.

4 DISSEMINATION, EXPLOITATION AND STANDARDISATION

The content of this report can be used for the development of future procedures of Virtual Testing. The observations and findings are brought into the discussions within HBM4VT group in the EURONCAP context. Models of the elements of the reclined load case have been published on TUC repository (https://tuc-project.org/frontal-sled-reclined/) together with experimental data provided by University of Virginia and Autoliv.

Concepts and findings described in this report have been included in publications at carhs CAE Grand Challenge, VDI Vehicle Safety Conference, Aachen Body Engineering Days and IRCOBI.

5 CONCLUSIONS

Following the distinction of several phases in a VT Virtual Testing process as proposed within IMVITER, HBM-based VT as the only procedure used in a homologation/assessment should involve three phases. While the first Phase serves internal model development by the OEM (which is comparable to what is done without VT), the second phase focuses on providing prove of the validity of the models. Calibrating models is not acceptable in this phase. The selection of appropriate validation tests, requirements to choose or define an appropriate validation device, were proposed including the specification of relevant validation channels.

The proposal was discussed related to the OSCCAR homologation test case, which consists of an occupant in a reclined seating position. For this new load case a validation procedure based on sled testing with the available THOR ATD was analysed and discussed. A set of validation channels was also proposed. The selection procedure for validation channels can also be applied to other HBM load cases in the future.

First ideas and concepts how to address scatter to define reasonable admittance criteria were developed. Proposals were made how to address scatter in a validation procedure. Based on that, an objective two-stage acceptance approach for vehicle environment certification is proposed. This approach was successfully applied to the OSCCAR validation load case.

The use of active HBMs will become of higher importance in the future. It is therefore essential to provide experimental data for this kind of modelling in order to validate. The indications given in this report on volunteer testing may serve as guidelines for researchers contributing to the creation of such data.

HBMs need further attendance in terms of validation for new seating positions associated to automated driving. New experimental campaigns are currently on their way to provide new data. The first available set of data in this context of full-scale experiments has been addressed in OSCCAR. With the description and overview on the model components of the experimental setup of reclined sled tests, guidance and orientation is given together with public access of the models.

Similarly, the pre-crash phase requires the validation of HBMs with respect to volunteer test data. Recommendations were formulated on the future acquisition of such data.

Modelling the load cases is usually done in more than one crash code. It is therefore important to derive recommendations for easing the multi-code modelling as much as possible. Such recommendations have been given in this report.

Preparing an HBM for the application in VT or for the simulation of validation load cases requires the definition of anthropometry and position. Objective approaches have been described in this report on reference point identification for this purpose.

A naming convention for these points, which is also in line with existing standards in this field, has been developed and exercised on a large number of proposed points.

The concepts described here will need further evaluation and refinement. Eventually, they should serve as a basis for future VT related activities and implementation in regulatory or consumer testing.

6 REFERENCES

[1] A. e. a. Eggers, “OSCCAR Deliverable D5.1 - Standardised procedure for validating a vehicle environment for VT,” www.osccarproject.eu

[2] *The VIVA OpenHBM finite element 50th percentile female occupant model: whole body model development and kinematic validation*, 2017. [Online]. Available: http://publications.lib.chalmers.se/records/fulltext/252248/local_252248.pdf

[3] C. Gehre and Gades H. and Wernicke, P., “Objective Rating of Signals Using Test and Simulation Responses,” *21st ESV Conference*.

[4] vetter, “ISO_TS13499_RED_B_162p2,”

[5] Julia Mühlbauer, Therese Fuchs, Katrin Brodbeck, Steffen Peldschus, “Reference points for a standardised application of Finite-Element Human Body Models in crash simulation,” in *World Congress of Biomechanics 2018*.

[6] THUMS User Community, *a project of LMU in cooperation with AUDI AG, Autoliv, BMW AG, Daimler AG, Dr. Ing. h. c. F. Porsche AG, ToyotaMotorCorporation, VolkswagenAG and ZFTRW.* [Online]. Available: https://tuc-project.org/

[7] *The Physiology of the Joints: Dépouillement v. 1 Upper limb. _ v. 2 Lower limb. _ v. 3 The trunk and the vertebral column*, 1970.

[8] G. Wu *et al.,* “ISB recommendation on definitions of joint coordinate systems of various joints for the reporting of human joint motion—Part II: shoulder, elbow, wrist and hand,” *Journal of Biomechanics*, vol. 38, no. 5, pp. 981–992, 2005, doi: 10.1016/j.jbiomech.2004.05.042.

[9] R. Baker, “ISB recommendation on definition of joint coordinate systems for the reporting of human joint motion—part I: ankle, hip and spine,” *Journal of Biomechanics*, vol. 36, no. 2, pp. 300–302, 2003, doi: 10.1016/s0021-9290(02)00336-6.

[10] D. Draper, A. Shah, S. Peldschus, and B. D. Stemper, “Initial validation of a human body model lumbar spine using dynamic compression,” in 2020. [Online]. Available: https://wbldb.lievers.net/10248440.html

[11] Nikolas Pfeiffer, “Automatisierte Erhebung von Metadaten für die Positionierung von numerischen Menschmodellen in der Crashsimulation,” Bachelorarbeit, Insitut für Informatik, Ludwig-Maximilians-Universität, München, 2019.

[12] I. Kasa, “A circle fitting procedure and its error analysis,” *IEEE Trans. Instrum. Meas.*, IM-25, no. 1, pp. 8–14, 1976, doi: 10.1109/tim.1976.6312298.

[13] V. J. Lumelsky, “On fast computation of distance between line segments,” *Information Processing Letters*, vol. 21, no. 2, pp. 55–61, 1985, doi: 10.1016/0020-0190(85)90032-8.

[14] Jérôme Uriot *et al.,* “Reference PMHS Sled Tests to Assess Submarining,” SAE Technical Paper 2015-22-0008, Nov. 2015. [Online]. Available: https://www.sae.org/publications/technical-papers/content/2015-22-0008/

[15] R. Richardson *et al.,* “Kinematic and Injury Response of Reclined PMHS in Frontal Impacts,” in *SAE Technical Paper Series*, 400 Commonwealth Drive, Warrendale, PA, United States, 2021. [Online]. Available: http://dx.doi.org/10.4271/2020-22-0004

[16] *A new generic frontal occupant sled test set-up developed within the EU-project SENIORS*, 2017. [Online]. Available: https://www-esv.nhtsa.dot.gov/proceedings/25/25esv-000261.pdf

[17] Greg Shaw, Dan Parent, Sergey Purtsezov, David Lessley, and Peter Martin, “Impact response of restrained PMHS in frontal sled tests: Skeletal deformation patterns under seat belt loading,” *Stapp Car Crash Journal*, vol. 53, pp. 1–48, 2009. [Online]. Available: https://www.researchgate.net/profile/stephen-ridella/publication/40896437_impact_response_of_restrained_pmhs_in_frontal_sled_tests_skeletal_deformation_patterns_under_seat_belt_loading

A. APPENDIX – NAMING CONVENTION

Table 6 to Table 13 show common landmarks and their identifiers according to the new naming convention code.

ID accoding to new naming convention	Landmark name	Piper Synonyms	Comments
head			
SKULL0AM	Left Porion/EAM		Long term additional Main location EXAM
SKULR0AM	Right Porion/EAM		
SKULL00R	Left Orbitale		long-term additional Main-location ORBI
SKULR00R	Right Orbitale		
SKULX0CG	Cranium center of gravity		
HEADX0CG	Head center of gravity		
SKULXR00	Skull back (PIPER)		
SKULXIR0	External_occipital_protuberance (PIPER)	LMK_SOP, Skull_SOP	
SKULLL00	Skull_lateral_left (PIPER)		
SKULRL00	Skull_lateral_right (PIPER)		
SKULXT00	Skull top (PIPER)		
SKULLF00	Infraorbital_Foramen_L	LMK_SIF_L	
SKULRF00	Infraorbital_Foramen_R	LMK_SIF_R	
SKULLIRL	Left_mastoid_process	LMK_SMP_L, Skull_SMP_L	
SKULRIRL	Right_mastoid_process	LMK_SMP_R, Skull_SMP_R	
SKULXF00	Anterior_nasal_spine	LMK_SNS	
SKULXIR0	Center_atlanto_occipital_joint	LMK_JIC	
HEADXSF0	Glabella	LMK_SGL	

SKULXSF0	Nasion	LMK_SNA	
SKULLFL0	Zygomatic_Angle_L	LMK_SZA_L	
SKULRFL0	Zygomatic_Angle_R	LMK_SZA_R	
SKULLIL0	Left_jaw_angle	LMK_JAN_L, Jaw_Angle_L	
SKULRIL0	Right_jaw_angle	LMK_JAN_R, Jaw_Angle_R	
SKULXIF0	Mental_protuberance_of_the_jaw	LMK_JMP	
SKULXIF1	Incisive	LMK_JIN	
SKULXIF2	Inferior_crest_of_the_jaw	LMK_JIC	

Table 6 Common head landmarks and corresponding code according to Naming Convention

ID accoding to new naming convention	Landmark name	Piper Synonyms	Comments
Upper body			
CLAVLL00	Left Clavicle lateral		
CLAVRL00	Right Clavicle lateral		
CLAVLM00	Left Clavicle medial		
CLAVRM00	Right Clavicle medial		
CLAVLFL0	Anterior_concavity_of_the_Clavicle_L		
CLAVRFL0	Anterior_concavity_of_the_Clavicle_R		
STRNLTL0	Upper edge of the concave of the left clavicular surface		
STRNRTL0	Upper edge of the concave of the right clavicular surface		
CLAVLFM0	Anterior convexity of the left clavicle	Clavicle_CAE_L	
CLAVRFM0	Anterior convexity of the right clavicle	Clavicle_CAE_R	
CLAVLMCR	Sternoclavicular joint of the left clavicle	Clavicle_CSJ_L	

CLAVRMCR	Sternoclavicular joint of the right clavicle	Clavicle_CSJ_R	
STRNLTCR	Left_sternum_sternoclavicular_joint		
STRNRTCR	Right_sternum_sternoclavicular_joint		
CLAVLRL0	Dorsal_point_of_left_acromioclavicular_joint		
CLAVRRL0	Dorsal_point_of_right_acromioclavicular_joint		
CLAVLLCR	Left_clavicle_acromioclavicular_joint		
CLAVRLCR	Right_clavicle_acromioclavicular_joint		
ACROLMCR	Acromioclavicular_joint_L	LMK_SAJ_L	
ACRORMCR	Acromioclavicular_joint_R	LMK_SAJ_R	
CLAVLFM1	Ventral_point_of_left_sternoclavicular_joint	LMK_CAS_L, Ventral_point_of_sternoclavicular_joint_L, Clavicle_CAS_L, SC_L	
CLAVRFM1	Ventral_point_of_right_sternoclavicular_joint	LMK_CAS_R, Ventral_point_of_sternoclavicular_joint_R, Clavicle_CAS_R, SC_R	
SCAPLRL0	Angulus_acromialis_of_left_scapula	L_Scapula_AA	
SCAPRRL0	Angulus_acromialis_of_right_scapula	R_Scapula_AA	
SCAPLRM0	Trigonum_spinae_of_left_scapula	Trigonum_spinae_of_scapula_L, TS_L	
SCAPRRM0	Trigonum_spinae_of_right_scapula	Trigonum_spinae_of_scapula_R, TS_R	
SCAPLI00	Angulus_inferior_of_left_scapula	L_Scapula_AI	
SCAPRI00	Angulus_inferior_of_rigth_scapula	R_Scapula_AI	
ACROLSFL	Acromial_tip_L	LMK_SAT_L	
ACRORSFL	Acromial_tip_R	LMK_SAT_R	

SCAPLSM0	Superior_angle_of_left_scapula	SSA_L	
SCAPRSM0	Superior_angle_of_right_scapula	SSA_R	
SCAPLLCR	Center_of_scapular_articulated_surface_to_the_left_humerus	rotule_scapula_L	
SCAPRLCR	Center_of_scapular_articulated_surface_to_the_right_humerus	rotule_scapula_R	
STRNXS00	suprasternal notch, Suprasternale		
STRNXICR	Substernale_(xyphoid_process)	LMK_SXS	
STRNLXXL	Left_point_on_the_middle_section_of_the_sternum		
STRNRXXL	Right_point_on_the_middle_section_of_the_sternum		
STRNXSCR	Manubriosternal_joint	LMK_SME	
RIBS01LA - RIBS12LA	Anterior extremity oft he left rib (rib 1-12)		
RIBS01RA - RIBS12RA	Anterior extremity oft he right rib (rib 1-12)		
RIBS01LL - RIBS10LL	Lateral left rib 1-10		
RIBS01RL - RIBS10RL	Lateral right rib 1-10		
RIBS01LP - RIBS12LP	Posterior extremity of the left rib (rib 1 -12)		
RIBS01RP - RIBS12RP	Posterior extremity of the right rib (rib 1 -12)		

Table 7 Common upper body landmarks and corresponding code according to naming convention

ID accoding to new naming convention	Landmark name	Piper Synonyms	Comments
Upper Extremities			
RADILDR0	styloid_process_of_left_radius	Styloid_process_of_radius_L, Radius_RSP_L, RS_L	
RADIRDR0	styloid_process_of_right_radius	Styloid_process_of_radius_R, Radius_RSP_R, RS_R	
RADILDU0	Sigmoid_notch_of_left_radius	Sigmoid_notch_of_radius_L, Radius_RUN_L	
RADIRDU0	Sigmoid_notch_of_right_radius	Sigmoid_notch_of_radius_R, Radius_RUN_R	
RADILPCR	elbow_joint_radius_L		
RADIRPCR	elbow_joint_radius_R		
RADILPXX	Center_depression_of_left_radial_head	Center_depression_of_radial_head_L, Radius_RHE_L	
RADIRPXX	Center_depression_of_right_radial_head	Center_depression_of_radial_head_R, Radius_RHE_R	
RADILDB0	Dorsal_tubercule_of_left_radius	Dorsal_tubercule_of_radius_L, Radius_RDT_L	
RADIRDB0	Dorsal_tubercule_of_right_radius	Dorsal_tubercule_of_radius_R, Radius_RDT_R	

HUMSLDL0	Lateral_epicondyle_of_left_humerus	Lateral_epicondyle_of_humerus_L, Humerus_HLE_L, EL_L	
HUMSRDL0	Lateral_epicondyle_of_right_humerus	Lateral_epicondyle_of_humerus_R, Humerus_HLE_R, EL_R	
HUMSLDM0	Medial_epicondyle_of_left_humerus	Medial_epicondyle_of_humerus_L, Humerus_HME_L, EM_L	
HUMSRDM0	Medial_epicondyle_of_right_humerus	Medial_epicondyle_of_humerus_R, Humerus_HME_R, EM_R	
ELBJL0CR	L_Humerus_MP_EL_EM		
ELBJR0CR	R_Humerus_MP_EL_EM		
WRISL0CR	L_wrist_MP_RS_US		
WRISR0CR	R_wrist_MP_RS_US		
HUMSLPCR	Head_center_of_left_humerus	Head_center_of_humerus_L, GH_L	
HUMSRPCR	Head_center_of_right_humerus	Head_center_of_humerus_R, GH_R	
HUMSLPL0	Greater_tubercle_of_the_left_humerus	HGT_L, Humerus_HGT_L	
HUMSRPL0	Greater_tubercle_of_the_right_humerus	HGT_R, Humerus_HGT_R	
ULNALD00	L_Ulna_US, Styloid_process_of_left_ulna	Styloid_process_of_ulnar_L, Ulna_USP_L, US_L	

ULNARD00	R_Ulna_US, Styloid_process_of_right_ulna	Styloid_process_of_ulnar_R, Ulna_USP_R, US_R	
ULNALPU0	Lateral_aspect_of_olecranon_of_the_left_ulna	UOL_L, Ulna_UOL_L	
ULNARPU0	Lateral_aspect_of_olecranon_of_the_right_ulna	UOL_R, Ulna_UOL_R	
ULNALPI0	Coronoid process of left ulna	Ulna_UCP_L	
ULNARPI0	Coronoid process of right ulna	Ulna_UCP_R	
ULNALPB0	Olecranon_apex_of_the_left_ulna	Ulna_UOA_L	
ULNARPB0	Olecranon_apex_of_the_right_ulna	Ulna_UOA_R	

Table 8 Common upper extremity landmarks and corresponding code according to naming convention

ID accoding to new naming convention	Landmark name	Piper Synonyms	Comments
Cervical Spine			
CESP03VC	Anterior_midpoint_of_the_body_of_C3		
CESP04VC	Anterior_midpoint_of_the_body_of_C4		
CESP05VC	Anterior_midpoint_of_the_body_of_C5		
CESP06VC	Anterior_midpoint_of_the_body_of_C6		
CESP07VC	Anterior_midpoint_of_the_body_of_C7		
CESP02BA	Anterior_point_of_the_inferior_plate_of_C2	LMK_C2LowerFrontEnd	
CESP03BA	Anterior_point_of_the_inferior_plate_of_C3	LMK_C3LowerFrontEnd	

CESP04BA	Anterior_point_of_the_inferior_plate_of_C4	LMK_C4LowerFrontEnd	
CESP05BA	Anterior_point_of_the_inferior_plate_of_C5	LMK_C5LowerFrontEnd	
CESP06BA	Anterior_point_of_the_inferior_plate_of_C6	LMK_C6LowerFrontEnd	
CESP07BA	Anterior_point_of_the_inferior_plate_of_C7	LMK_C7LowerFrontEnd	
CESP03TA	Anterior_point_of_the_superior_plate_of_C3	VC3, LMK_C3UpperFrontEnd	
CESP04TA	Anterior_point_of_the_superior_plate_of_C4	VC4, LMK_C4UpperFrontEnd	
CESP05TA	Anterior_point_of_the_superior_plate_of_C5	VC5, LMK_C5UpperFrontEnd	
CESP06TA	Anterior_point_of_the_superior_plate_of_C6	VC6, LMK_C6UpperFrontEnd	
CESP07TA	Anterior_point_of_the_superior_plate_of_C7	VC7, LMK_C7UpperFrontEnd	
CESP02VC	Anterior_tuberosity_of_C2	LMK_C2AntArch	
CESP02BC	Center_lower_plate_of_C2		
CESP03BC	Center_lower_plate_of_C3	LMK_C3LowerMid	
CESP04BC	Center_lower_plate_of_C4	LMK_C4LowerMid	
CESP05BC	Center_lower_plate_of_C5	LMK_C5LowerMid	
CESP06BC	Center_lower_plate_of_C6	LMK_C6LowerMid	
CESP07BC	Center_lower_plate_of_C7	LMK_C7LowerMid	
CESP02TC	Center_upper_plate_of_C2		
CESP03TC	Center_upper_plate_of_C3	LMK_C3UpperMid	
CESP04TC	Center_upper_plate_of_C4	LMK_C4UpperMid	

CESP05TC	Center_upper_plate_of_C5	LMK_C5UpperMid	
CESP06TC	Center_upper_plate_of_C6	LMK_C6UpperMid	
CESP07TC	Center_upper_plate_of_C7	LMK_C7UpperMid	
CESP01CG	C1_COG		
CESP01CE	C1_center		
CESP02CG	C2_COG		
CESP02CE	C2_center		
CESP03CG	C3_COG		
CESP03CE	C3_center		
CESP04CG	C4_COG		
CESP04CE	C4_center		
CESP05CG	C5_COG		
CESP05CE	C5_center		
CESP06CG	C6_COG		
CESP06CE	C6_center		
CESP07CG	C7_COG		
CESP07CE	C7_center		
CESP03LT	LMK_C3TransProc_L	LMK_C3TransProc_L	
CESP03RT	LMK_C3TransProc_R	LMK_C3TransProc_R	
CESP04LT	LMK_C4TransProc_L	LMK_C4TransProc_L	
CESP04RT	LMK_C4TransProc_R	LMK_C4TransProc_R	
CESP05LT	LMK_C5TransProc_L	LMK_C5TransProc_L	
CESP05RT	LMK_C5TransProc_R	LMK_C5TransProc_R	

CESP06LT	LMK_C6TransProc_L	LMK_C6TransProc_L	
CESP06RT	LMK_C6TransProc_R	LMK_C6TransProc_R	
CESP07LT	LMK_C7TransProc_L	LMK_C7TransProc_L	
CESP07RT	LMK_C7TransProc_R	LMK_C7TransProc_R	
CESP03LC	Left_midpoint_of_the_body_of_C3		
CESP04LC	Left_midpoint_of_the_body_of_C4		
CESP05LC	Left_midpoint_of_the_body_of_C5		
CESP06LC	Left_midpoint_of_the_body_of_C6		
CESP07LC	Left_midpoint_of_the_body_of_C7		
CESP02BL	Left_point_of_the_inferior_plate_of_C2	LMK_C2LowerLeftEnd	
CESP03BL	Left_point_of_the_inferior_plate_of_C3	LMK_C3LowerLeftEnd	
CESP04BL	Left_point_of_the_inferior_plate_of_C4	LMK_C4LowerLeftEnd	
CESP05BL	Left_point_of_the_inferior_plate_of_C5	LMK_C5LowerLeftEnd	
CESP06BL	Left_point_of_the_inferior_plate_of_C6	LMK_C6LowerLeftEnd	
CESP07BL	Left_point_of_the_inferior_plate_of_C7	LMK_C7LowerLeftEnd	
CESP03TL	Left_point_of_the_superior_plate_of_C3	LMK_C3UpperLeftEnd	
CESP04TL	Left_point_of_the_superior_plate_of_C4	LMK_C4UpperLeftEnd	
CESP05TL	Left_point_of_the_superior_plate_of_C5	LMK_C5UpperLeftEnd	
CESP06TL	Left_point_of_the_superior_plate_of_C6	LMK_C6UpperLeftEnd	

CESP07TL	Left_point_of_the_superior_plate_of_C7	LMK_C7UpperLeft End	
CESP01PR	Right_tip_of_the_spinous_process_of_C1	LMK_C2Spinous_R, CV2_1	
CESP03PR	Right_tip_of_the_spinous_process_of_C3	LMK_C3Spinous_R, CV3_1	
CESP04PR	Right_tip_of_the_spinous_process_of_C4	LMK_C4Spinous_R, CV4_1	
CESP05PR	Right_tip_of_the_spinous_process_of_C5	LMK_C5Spinous_R, CV5_1	
CESP06PR	Right_tip_of_the_spinous_process_of_C6	LMK_C6Spinous_R, CV6_1	
CESP03PS	Superior_point_of_tip_of_spinous_process_of_C3	DC3	
CESP04PS	Superior_point_of_tip_of_spinous_process_of_C4	DC4	
CESP05PS	Superior_point_of_tip_of_spinous_process_of_C5	DC5	
CESP06PS	Superior_point_of_tip_of_spinous_process_of_C6	DC6	
CESP07PS	Superior_point_of_tip_of_spinous_process_of_C7	DC7	
CESP02PP	Most_posterior_point_of_tip_of_spinous_process_of_C2		
CESP03PP	Most_posterior_point_of_tip_of_spinous_process_of_C3		
CESP04PP	Most_posterior_point_of_tip_of_spinous_process_of_C4		
CESP05PP	Most_posterior_point_of_tip_of_spinous_process_of_C5		
CESP06PP	Most_posterior_point_of_tip_of_spinous_process_of_C6		
CESP07PP	Most_posterior_point_of_tip_of_spinous_process_of_C7		

CESP01VC	Tuberosity_of_the_anterior_arch_of_C1		
CESP02DT	Tip_of_the_odeontoid/dens_of_C2		
CESP03DC	Posterior_midpoint_of_the_body_of_C3		
CESP04DC	Posterior_midpoint_of_the_body_of_C4		
CESP05DC	Posterior_midpoint_of_the_body_of_C5		
CESP06DC	Posterior_midpoint_of_the_body_of_C6		
CESP07DC	Posterior_midpoint_of_the_body_of_C7		
CESP02BP	Posterior_point_of_the_inferior_plate_of_C2	LMK_C2LowerRearEnd	
CESP03BP	Posterior_point_of_the_inferior_plate_of_C3	LMK_C3LowerRearEnd	
CESP04BP	Posterior_point_of_the_inferior_plate_of_C4	LMK_C4LowerRearEnd	
CESP05BP	Posterior_point_of_the_inferior_plate_of_C5	LMK_C5LowerRearEnd	
CESP06BP	Posterior_point_of_the_inferior_plate_of_C6	LMK_C6LowerRearEnd	
CESP07BP	Posterior_point_of_the_inferior_plate_of_C7	LMK_C7LowerRearEnd	
CESP03TP	Posterior_point_of_the_superior_plate_of_C3	LMK_C3UpperRearEnd	
CESP04TP	Posterior_point_of_the_superior_plate_of_C4	LMK_C4UpperRearEnd	
CESP05TP	Posterior_point_of_the_superior_plate_of_C5	LMK_C5UpperRearEnd	
CESP06TP	Posterior_point_of_the_superior_plate_of_C6	LMK_C6UpperRearEnd	
CESP07TP	Posterior_point_of_the_superior_plate_of_C7	LMK_C7UpperRearEnd	
CESP03RC	Right_midpoint_of_the_body_of_C3		
CESP04RC	Right_midpoint_of_the_body_of_C4		

CESP05RC	Right_midpoint_of_the_body_of_C5		
CESP06RC	Right_midpoint_of_the_body_of_C6		
CESP07RC	Right_midpoint_of_the_body_of_C7		
CESP02BR	Right_point_of_the_inferior_plate_of_C2	LMK_C2LowerRightEnd	
CESP03BR	Right_point_of_the_inferior_plate_of_C3	LMK_C3LowerRightEnd	
CESP04BR	Right_point_of_the_inferior_plate_of_C4	LMK_C4LowerRightEnd	
CESP05BR	Right_point_of_the_inferior_plate_of_C5	LMK_C5LowerRightEnd	
CESP06BR	Right_point_of_the_inferior_plate_of_C6	LMK_C6LowerRightEnd	
CESP07BR	Right_point_of_the_inferior_plate_of_C7	LMK_C7LowerRightEnd	
CESP03TR	Right_point_of_the_superior_plate_of_C3	LMK_C3UpperRightEnd	
CESP04TR	Right_point_of_the_superior_plate_of_C4	LMK_C4UpperRightEnd	
CESP05TR	Right_point_of_the_superior_plate_of_C5	LMK_C5UpperRightEnd	
CESP06TR	Right_point_of_the_superior_plate_of_C6	LMK_C6UpperRightEnd	
CESP07TR	Right_point_of_the_superior_plate_of_C7	LMK_C7UpperRightEnd	

Table 9 Common cervical spine landmarks and corresponding code according to naming convention

ID accoding to new naming convention	Landmark name	Piper Synonyms	Comments
Thoracal Spine			
THSP01LC	Left_midpoint_of_the_body_of_T1		

THSP01RC	Right_midpoint_of_the_body_of_T1		
THSP08LC	Left_midpoint_of_the_body_of_T8		
THSP08RC	Right_midpoint_of_the_body_of_T8		
THSP11LC	Left_midpoint_of_the_body_of_T11		
THSP11RC	Right_midpoint_of_the_body_of_T11		
THSP01VC	Anterior_midpoint_of_the_body_of_T1		
THSP02VC	Anterior_midpoint_of_the_body_of_T2		
THSP03VC	Anterior_midpoint_of_the_body_of_T3		
THSP04VC	Anterior_midpoint_of_the_body_of_T4		
THSP05VC	Anterior_midpoint_of_the_body_of_T5		
THSP06VC	Anterior_midpoint_of_the_body_of_T6		
THSP07VC	Anterior_midpoint_of_the_body_of_T7		
THSP08VC	Anterior_midpoint_of_the_body_of_T8		
THSP09VC	Anterior_midpoint_of_the_body_of_T9		
THSP10VC	Anterior_midpoint_of_the_body_of_T10		
THSP11VC	Anterior_midpoint_of_the_body_of_T11		
THSP12VC	Anterior_midpoint_of_the_body_of_T12		
THSP01DC	Posterior_midpoint_of_the_body_of_T1		
THSP02DC	Posterior_midpoint_of_the_body_of_T2		
THSP03DC	Posterior_midpoint_of_the_body_of_T3		
THSP04DC	Posterior_midpoint_of_the_body_of_T4		
THSP05DC	Posterior_midpoint_of_the_body_of_T5		
THSP06DC	Posterior_midpoint_of_the_body_of_T6		
THSP07DC	Posterior_midpoint_of_the_body_of_T7		
THSP08DC	Posterior_midpoint_of_the_body_of_T8		
THSP09DC	Posterior_midpoint_of_the_body_of_T9		

THSP10DC	Posterior_midpoint_of_the_body_of_T10		
THSP11DC	Posterior_midpoint_of_the_body_of_T11		
THSP12DC	Posterior_midpoint_of_the_body_of_T12		
THSP01BA	Anterior_point_of_the_inferior_plate_of_T1	LMK_T01LowerFrontEnd	
THSP02BA	Anterior_point_of_the_inferior_plate_of_T2	LMK_T02LowerFrontEnd	
THSP03BA	Anterior_point_of_the_inferior_plate_of_T3	LMK_T03LowerFrontEnd	
THSP04BA	Anterior_point_of_the_inferior_plate_of_T4	LMK_T04LowerFrontEnd	
THSP05BA	Anterior_point_of_the_inferior_plate_of_T5	LMK_T05LowerFrontEnd	
THSP06BA	Anterior_point_of_the_inferior_plate_of_T6	LMK_T06LowerFrontEnd	
THSP07BA	Anterior_point_of_the_inferior_plate_of_T7	LMK_T07LowerFrontEnd	
THSP08BA	Anterior_point_of_the_inferior_plate_of_T8	LMK_T08LowerFrontEnd	
THSP09BA	Anterior_point_of_the_inferior_plate_of_T9	LMK_T09LowerFrontEnd	
THSP10BA	Anterior_point_of_the_inferior_plate_of_T10	LMK_T10LowerFrontEnd	
THSP11BA	Anterior_point_of_the_inferior_plate_of_T11	LMK_T11LowerFrontEnd	
THSP12BA	Anterior_point_of_the_inferior_plate_of_T12	LMK_T12LowerFrontEnd	
THSP01TA	Anterior_point_of_the_superior_plate_of_T1	VT01, LMK_T01UpperFrontEnd	
THSP02TA	Anterior_point_of_the_superior_plate_of_T2	VT02, LMK_T02UpperFrontEnd	

THSP03TA	Anterior_point_of_the_superior_plate_of_T3	VT03, LMK_T03UpperFrontEnd	
THSP04TA	Anterior_point_of_the_superior_plate_of_T4	VT04, LMK_T04UpperFrontEnd	
THSP05TA	Anterior_point_of_the_superior_plate_of_T5	VT05, LMK_T05UpperFrontEnd	
THSP06TA	Anterior_point_of_the_superior_plate_of_T6	VT06, LMK_T06UpperFrontEnd	
THSP07TA	Anterior_point_of_the_superior_plate_of_T7	VT07, LMK_T07UpperFrontEnd	
THSP08TA	Anterior_point_of_the_superior_plate_of_T8	VT08, LMK_T08UpperFrontEnd	
THSP09TA	Anterior_point_of_the_superior_plate_of_T9	VT09, LMK_T09UpperFrontEnd	
THSP10TA	Anterior_point_of_the_superior_plate_of_T10	VT10, LMK_T10UpperFrontEnd	
THSP11TA	Anterior_point_of_the_superior_plate_of_T11	VT11, LMK_T11UpperFrontEnd	
THSP12TA	Anterior_point_of_the_superior_plate_of_T12	VT12, LMK_T12UpperFrontEnd	
THSP01BC	T1_bottom		
THSP02BC	T2_bottom	LMK_T02LowerMid	
THSP03BC	T3_bottom	LMK_T03LowerMid	
THSP04BC	T4_bottom	LMK_T04LowerMid	
THSP05BC	T5_bottom	LMK_T05LowerMid	
THSP06BC	T6_bottom	LMK_T06LowerMid	

THSP07BC	T7_bottom	LMK_T07LowerMid	
THSP08BC	T8_bottom	LMK_T08LowerMid	
THSP09BC	T9_bottom	LMK_T09LowerMid	
THSP10BC	T10_bottom	LMK_T10LowerMid	
THSP11BC	T11_bottom	LMK_T11LowerMid	
THSP12BC	T12_bottom	LMK_T12LowerMid	
THSP01TC	T1_top	LMK_T01UpperMid	
THSP02TC	T2_top	LMK_T02UpperMid	
THSP03TC	T3_top	LMK_T03UpperMid	
THSP04TC	T4_top	LMK_T04UpperMid	
THSP05TC	T5_top	LMK_T05UpperMid	
THSP06TC	T6_top	LMK_T06UpperMid	
THSP07TC	T7_top	LMK_T07UpperMid	
THSP08TC	T8_top	LMK_T08UpperMid	
THSP09TC	T9_top	LMK_T09UpperMid	
THSP10TC	T10_top	LMK_T10UpperMid	
THSP11TC	T11_top	LMK_T11UpperMid	
THSP12TC	T12_top	LMK_T12UpperMid	
THSP01CG	T1_COG		
THSP01CE	T1_center		
THSP02CG	T2_COG		
THSP02CE	T2_center		
THSP03CG	T3_COG		
THSP03CE	T3_center		
THSP04CG	T4_COG		
THSP04CE	T4_center		

THSP05CG	T5_COG		
THSP05CE	T5_center		
THSP06CG	T6_COG		
THSP06CE	T6_center		
THSP07CG	T7_COG		
THSP07CE	T7_center		
THSP08CG	T8_COG		
THSP08CE	T8_center		
THSP09CG	T9_COG		
THSP09CE	T9_center		
THSP10CG	T10_COG		
THSP10CE	T10_center		
THSP11CG	T11_COG		
THSP11CE	T11_center		
THSP12CG	T12_COG		
THSP12CE	T12_center		
THSP01PI	Inferior_point_of_tip_of_spinous_process_of_T1	LMK_TV01	
THSP02PI	Inferior_point_of_tip_of_spinous_process_of_T2	LMK_TV02	
THSP03PI	Inferior_point_of_tip_of_spinous_process_of_T3	LMK_TV03	
THSP04PI	Inferior_point_of_tip_of_spinous_process_of_T4	LMK_TV04	
THSP05PI	Inferior_point_of_tip_of_spinous_process_of_T5	LMK_TV05	
THSP06PI	Inferior_point_of_tip_of_spinous_process_of_T6	LMK_TV06	

THSP07PI	Inferior_point_of_tip_of_spinous_process_of_T7	LMK_TV07	
THSP08PI	Inferior_point_of_tip_of_spinous_process_of_T8	LMK_TV08	
THSP09PI	Inferior_point_of_tip_of_spinous_process_of_T9	LMK_TV09	
THSP10PI	Inferior_point_of_tip_of_spinous_process_of_T10	LMK_TV10	
THSP11PI	Inferior_point_of_tip_of_spinous_process_of_T11	LMK_TV11	
THSP12PI	Inferior_point_of_tip_of_spinous_process_of_T12	LMK_TV12	
THSP01PS	Superior_point_of_tip_of_spinous_process_of_T1	DT01	
THSP02PS	Superior_point_of_tip_of_spinous_process_of_T2	DT02	
THSP03PS	Superior_point_of_tip_of_spinous_process_of_T3	DT03	
THSP04PS	Superior_point_of_tip_of_spinous_process_of_T4	DT04	
THSP05PS	Superior_point_of_tip_of_spinous_process_of_T5	DT05	
THSP06PS	Superior_point_of_tip_of_spinous_process_of_T6	DT06	
THSP07PS	Superior_point_of_tip_of_spinous_process_of_T7	DT07	
THSP08PS	Superior_point_of_tip_of_spinous_process_of_T8	DT08	
THSP09PS	Superior_point_of_tip_of_spinous_process_of_T9	DT09	
THSP10PS	Superior_point_of_tip_of_spinous_process_of_T10	DT10	
THSP11PS	Superior_point_of_tip_of_spinous_process_of_T11	DT11	

THSP12PS	Superior_point_of_tip_of_spinous_process_of_T12	DT12	
THSP01LT	LMK_T01TransProc_L	LMK_T01TransProc_L	
THSP01RT	LMK_T01TransProc_R	LMK_T01TransProc_R	
THSP02LT	LMK_T02TransProc_L	LMK_T02TransProc_L	
THSP02RT	LMK_T02TransProc_R	LMK_T02TransProc_R	
THSP03LT	LMK_T03TransProc_L	LMK_T03TransProc_L	
THSP03RT	LMK_T03TransProc_R	LMK_T03TransProc_R	
THSP04LT	LMK_T04TransProc_L	LMK_T04TransProc_L	
THSP04RT	LMK_T04TransProc_R	LMK_T04TransProc_R	
THSP05LT	LMK_T05TransProc_L	LMK_T05TransProc_L	
THSP05RT	LMK_T05TransProc_R	LMK_T05TransProc_R	
THSP06LT	LMK_T06TransProc_L	LMK_T06TransProc_L	
THSP06RT	LMK_T06TransProc_R	LMK_T06TransProc_R	
THSP07LT	LMK_T07TransProc_L	LMK_T07TransProc_L	
THSP07RT	LMK_T07TransProc_R	LMK_T07TransProc_R	
THSP08LT	LMK_T08TransProc_L	LMK_T08TransProc_L	
THSP08RT	LMK_T08TransProc_R	LMK_T08TransProc_R	

THSP09LT	LMK_T09TransProc_L	LMK_T09TransProc_L	
THSP09RT	LMK_T09TransProc_R	LMK_T09TransProc_R	
THSP10LT	LMK_T10TransProc_L	LMK_T10TransProc_L	
THSP10RT	LMK_T10TransProc_R	LMK_T10TransProc_R	
THSP11LT	LMK_T11TransProc_L	LMK_T11TransProc_L	
THSP11RT	LMK_T11TransProc_R	LMK_T11TransProc_R	
THSP12LT	LMK_T12TransProc_L	LMK_T12TransProc_L	
THSP12RT	LMK_T12TransProc_R	LMK_T12TransProc_R	
THSP01LC	Left_midpoint_of_the_body_of_T1		
THSP02LC	Left_midpoint_of_the_body_of_T2		
THSP03LC	Left_midpoint_of_the_body_of_T3		
THSP04LC	Left_midpoint_of_the_body_of_T4		
THSP05LC	Left_midpoint_of_the_body_of_T5		
THSP06LC	Left_midpoint_of_the_body_of_T6		
THSP07LC	Left_midpoint_of_the_body_of_T7		
THSP08LC	Left_midpoint_of_the_body_of_T8		
THSP09LC	Left_midpoint_of_the_body_of_T9		
THSP10LC	Left_midpoint_of_the_body_of_T10		
THSP11LC	Left_midpoint_of_the_body_of_T11		
THSP12LC	Left_midpoint_of_the_body_of_T12		
THSP01RC	Right_midpoint_of_the_body_of_T1		
THSP02RC	Right_midpoint_of_the_body_of_T2		

THSP03RC	Right_midpoint_of_the_body_of_T3		
THSP04RC	Right_midpoint_of_the_body_of_T4		
THSP05RC	Right_midpoint_of_the_body_of_T5		
THSP06RC	Right_midpoint_of_the_body_of_T6		
THSP07RC	Right_midpoint_of_the_body_of_T7		
THSP08RC	Right_midpoint_of_the_body_of_T8		
THSP09RC	Right_midpoint_of_the_body_of_T9		
THSP10RC	Right_midpoint_of_the_body_of_T10		
THSP11RC	Right_midpoint_of_the_body_of_T11		
THSP12RC	Right_midpoint_of_the_body_of_T12		
THSP01BL	Left_point_of_the_inferior_plate_of_T1	LMK_T01LowerLeftEnd	
THSP02BL	Left_point_of_the_inferior_plate_of_T2	LMK_T02LowerLeftEnd	
THSP03BL	Left_point_of_the_inferior_plate_of_T3	LMK_T03LowerLeftEnd	
THSP04BL	Left_point_of_the_inferior_plate_of_T4	LMK_T04LowerLeftEnd	
THSP05BL	Left_point_of_the_inferior_plate_of_T5	LMK_T05LowerLeftEnd	
THSP06BL	Left_point_of_the_inferior_plate_of_T6	LMK_T06LowerLeftEnd	
THSP07BL	Left_point_of_the_inferior_plate_of_T7	LMK_T07LowerLeftEnd	
THSP08BL	Left_point_of_the_inferior_plate_of_T8	LMK_T08LowerLeftEnd	
THSP09BL	Left_point_of_the_inferior_plate_of_T9	LMK_T09LowerLeftEnd	
THSP10BL	Left_point_of_the_inferior_plate_of_T10	LMK_T10LowerLeftEnd	

THSP11BL	Left_point_of_the_inferior_plate_of_T11	LMK_T11LowerLeftEnd	
THSP12BL	Left_point_of_the_inferior_plate_of_T12	LMK_T12LowerLeftEnd	
THSP01TL	Left_point_of_the_superior_plate_of_T1	LMK_T01UpperLeftEnd	
THSP02TL	Left_point_of_the_superior_plate_of_T2	LMK_T02UpperLeftEnd	
THSP03TL	Left_point_of_the_superior_plate_of_T3	LMK_T03UpperLeftEnd	
THSP04TL	Left_point_of_the_superior_plate_of_T4	LMK_T04UpperLeftEnd	
THSP05TL	Left_point_of_the_superior_plate_of_T5	LMK_T05UpperLeftEnd	
THSP06TL	Left_point_of_the_superior_plate_of_T6	LMK_T06UpperLeftEnd	
THSP07TL	Left_point_of_the_superior_plate_of_T7	LMK_T07UpperLeftEnd	
THSP08TL	Left_point_of_the_superior_plate_of_T8	LMK_T08UpperLeftEnd	
THSP09TL	Left_point_of_the_superior_plate_of_T9	LMK_T09UpperLeftEnd	
THSP10TL	Left_point_of_the_superior_plate_of_T10	LMK_T10UpperLeftEnd	
THSP11TL	Left_point_of_the_superior_plate_of_T11	LMK_T11UpperLeftEnd	
THSP12TL	Left_point_of_the_superior_plate_of_T12	LMK_T12UpperLeftEnd	
THSP01BP	Posterior_point_of_the_inferior_plate_of_T1	LMK_T01LowerRearEnd	
THSP02BP	Posterior_point_of_the_inferior_plate_of_T2	LMK_T02LowerRearEnd	
THSP03BP	Posterior_point_of_the_inferior_plate_of_T3	LMK_T03LowerRearEnd	

THSP04BP	Posterior_point_of_the_inferior_plate_of_T4	LMK_T04LowerRearEnd	
THSP05BP	Posterior_point_of_the_inferior_plate_of_T5	LMK_T05LowerRearEnd	
THSP06BP	Posterior_point_of_the_inferior_plate_of_T6	LMK_T06LowerRearEnd	
THSP07BP	Posterior_point_of_the_inferior_plate_of_T7	LMK_T07LowerRearEnd	
THSP08BP	Posterior_point_of_the_inferior_plate_of_T8	LMK_T08LowerRearEnd	
THSP09BP	Posterior_point_of_the_inferior_plate_of_T9	LMK_T09LowerRearEnd	
THSP10BP	Posterior_point_of_the_inferior_plate_of_T10	LMK_T10LowerRearEnd	
THSP11BP	Posterior_point_of_the_inferior_plate_of_T11	LMK_T11LowerRearEnd	
THSP12BP	Posterior_point_of_the_inferior_plate_of_T12	LMK_T12LowerRearEnd	
THSP01TP	Posterior_point_of_the_superior_plate_of_T1	LMK_T01UpperRearEnd	
THSP02TP	Posterior_point_of_the_superior_plate_of_T2	LMK_T02UpperRearEnd	
THSP03TP	Posterior_point_of_the_superior_plate_of_T3	LMK_T03UpperRearEnd	
THSP04TP	Posterior_point_of_the_superior_plate_of_T4	LMK_T04UpperRearEnd	
THSP05TP	Posterior_point_of_the_superior_plate_of_T5	LMK_T05UpperRearEnd	
THSP06TP	Posterior_point_of_the_superior_plate_of_T6	LMK_T06UpperRearEnd	
THSP07TP	Posterior_point_of_the_superior_plate_of_T7	LMK_T07UpperRearEnd	
THSP08TP	Posterior_point_of_the_superior_plate_of_T8	LMK_T08UpperRearEnd	

THSP09TP	Posterior_point_of_the_superior_plate_of_T9	LMK_T09UpperRearEnd	
THSP10TP	Posterior_point_of_the_superior_plate_of_T10	LMK_T10UpperRearEnd	
THSP11TP	Posterior_point_of_the_superior_plate_of_T11	LMK_T11UpperRearEnd	
THSP12TP	Posterior_point_of_the_superior_plate_of_T12	LMK_T12UpperRearEnd	
THSP01BR	Right_point_of_the_inferior_plate_of_T1	LMK_T01LowerRightEnd	
THSP02BR	Right_point_of_the_inferior_plate_of_T2	LMK_T02LowerRightEnd	
THSP03BR	Right_point_of_the_inferior_plate_of_T3	LMK_T03LowerRightEnd	
THSP04BR	Right_point_of_the_inferior_plate_of_T4	LMK_T04LowerRightEnd	
THSP05BR	Right_point_of_the_inferior_plate_of_T5	LMK_T05LowerRightEnd	
THSP06BR	Right_point_of_the_inferior_plate_of_T6	LMK_T06LowerRightEnd	
THSP07BR	Right_point_of_the_inferior_plate_of_T7	LMK_T07LowerRightEnd	
THSP08BR	Right_point_of_the_inferior_plate_of_T8	LMK_T08LowerRightEnd	
THSP09BR	Right_point_of_the_inferior_plate_of_T9	LMK_T09LowerRightEnd	
THSP10BR	Right_point_of_the_inferior_plate_of_T10	LMK_T10LowerRightEnd	
THSP11BR	Right_point_of_the_inferior_plate_of_T11	LMK_T11LowerRightEnd	
THSP12BR	Right_point_of_the_inferior_plate_of_T12	LMK_T12LowerRightEnd	
THSP01TR	Right_point_of_the_superior_plate_of_T1	LMK_T01UpperRightEnd	

THSP02TR	Right_point_of_the_superior_plate_of_T2	LMK_T02UpperRightEnd	
THSP03TR	Right_point_of_the_superior_plate_of_T3	LMK_T03UpperRightEnd	
THSP04TR	Right_point_of_the_superior_plate_of_T4	LMK_T04UpperRightEnd	
THSP05TR	Right_point_of_the_superior_plate_of_T5	LMK_T05UpperRightEnd	
THSP06TR	Right_point_of_the_superior_plate_of_T6	LMK_T06UpperRightEnd	
THSP07TR	Right_point_of_the_superior_plate_of_T7	LMK_T07UpperRightEnd	
THSP08TR	Right_point_of_the_superior_plate_of_T8	LMK_T08UpperRightEnd	
THSP09TR	Right_point_of_the_superior_plate_of_T9	LMK_T09UpperRightEnd	
THSP10TR	Right_point_of_the_superior_plate_of_T10	LMK_T10UpperRightEnd	
THSP11TR	Right_point_of_the_superior_plate_of_T11	LMK_T11UpperRightEnd	
THSP12TR	Right_point_of_the_superior_plate_of_T12	LMK_T12UpperRightEnd	

Table 10 Common thoracal spine landmarks and corresponding code according to naming convention

ID accoding to new naming convention	Landmark name	Piper Synonyms	Comments
Lumbar Spine			
LUSP01PS	Superior_point_of_tip_of_spinous_process_of_L1	DL1	
LUSP02PS	Superior_point_of_tip_of_spinous_process_of_L2	DL2	

LUSP03PS	Superior_point_of_tip_of_spinous_process_of_L3	DL3	
LUSP04PS	Superior_point_of_tip_of_spinous_process_of_L4	DL4	
LUSP05PS	Superior_point_of_tip_of_spinous_process_of_L5	DL5	
LUSP01PI	Inferior_point_of_tip_of_spinous_process_of_L1	LMK_LV1	
LUSP02PI	Inferior_point_of_tip_of_spinous_process_of_L2	LMK_LV2	
LUSP03PI	Inferior_point_of_tip_of_spinous_process_of_L3	LMK_LV3	
LUSP04PI	Inferior_point_of_tip_of_spinous_process_of_L4	LMK_LV4	
LUSP05PI	Inferior_point_of_tip_of_spinous_process_of_L5	LMK_LV5	
LUSP01LT	LMK_L1TransProc_L	Tip_of_left_transverse_process_of_L1	
LUSP01RT	LMK_L1TransProc_R	Tip_of_right_transverse_process_of_L1	
LUSP02LT	LMK_L2TransProc_L	Tip_of_left_transverse_process_of_L2	
LUSP02RT	LMK_L2TransProc_R	Tip_of_right_transverse_process_of_L2	
LUSP03LT	LMK_L3TransProc_L	Tip_of_left_transverse_process_of_L3	
LUSP03RT	LMK_L3TransProc_R	Tip_of_right_transverse_process_of_L3	
LUSP04LT	LMK_L4TransProc_L	Tip_of_left_transverse_process_of_L4	
LUSP04RT	LMK_L4TransProc_R	Tip_of_right_transverse_process_of_L4	

LUSP05LT	LMK_L5TransProc_L	Tip_of_left_transverse_process_of_L5	
LUSP05RT	LMK_L5TransProc_R	Tip_of_right_transverse_process_of_L5	
LUSP01LC	Left_midpoint_of_the_body_of_L1		
LUSP02LC	Left_midpoint_of_the_body_of_L2		
LUSP03LC	Left_midpoint_of_the_body_of_L3		
LUSP04LC	Left_midpoint_of_the_body_of_L4		
LUSP05LC	Left_midpoint_of_the_body_of_L5		
LUSP01RC	Right_midpoint_of_the_body_of_L1		
LUSP02RC	Right_midpoint_of_the_body_of_L2		
LUSP03RC	Right_midpoint_of_the_body_of_L3		
LUSP04RC	Right_midpoint_of_the_body_of_L4		
LUSP05RC	Right_midpoint_of_the_body_of_L5		
LUSP01BL	Left_point_of_the_inferior_plate_of_L1	LMK_L1LowerLeftEnd	
LUSP02BL	Left_point_of_the_inferior_plate_of_L2	LMK_L2LowerLeftEnd	
LUSP03BL	Left_point_of_the_inferior_plate_of_L3	LMK_L3LowerLeftEnd	
LUSP04BL	Left_point_of_the_inferior_plate_of_L4	LMK_L4LowerLeftEnd	
LUSP05BL	Left_point_of_the_inferior_plate_of_L5	LMK_L5LowerLeftEnd	
LUSP01TL	Left_point_of_the_superior_plate_of_L1	LMK_L1UpperLeftEnd	
LUSP02TL	Left_point_of_the_superior_plate_of_L2	LMK_L2UpperLeftEnd	
LUSP03TL	Left_point_of_the_superior_plate_of_L3	LMK_L3UpperLeftEnd	

LUSP04TL	Left_point_of_the_superior_plate_of_L4	LMK_L4UpperLeftEnd	
LUSP05TL	Left_point_of_the_superior_plate_of_L5	LMK_L5UpperLeftEnd	
LUSP01DC	Posterior_midpoint_of_the_body_of_L1		
LUSP02DC	Posterior_midpoint_of_the_body_of_L2		
LUSP03DC	Posterior_midpoint_of_the_body_of_L3		
LUSP04DC	Posterior_midpoint_of_the_body_of_L4		
LUSP05DC	Posterior_midpoint_of_the_body_of_L5		
LUSP01BP	Posterior_point_of_the_inferior_plate_of_L1	LMK_L1LowerRearEnd	
LUSP02BP	Posterior_point_of_the_inferior_plate_of_L2	LMK_L2LowerRearEnd	
LUSP03BP	Posterior_point_of_the_inferior_plate_of_L3	LMK_L3LowerRearEnd	
LUSP04BP	Posterior_point_of_the_inferior_plate_of_L4	LMK_L4LowerRearEnd	
LUSP05BP	Posterior_point_of_the_inferior_plate_of_L5	LMK_L5LowerRearEnd	
LUSP01TP	Posterior_point_of_the_superior_plate_of_L1	LMK_L1UpperRearEnd	
LUSP02TP	Posterior_point_of_the_superior_plate_of_L2	LMK_L2UpperRearEnd	
LUSP03TP	Posterior_point_of_the_superior_plate_of_L3	LMK_L3UpperRearEnd	
LUSP04TP	Posterior_point_of_the_superior_plate_of_L4	LMK_L4UpperRearEnd	
LUSP05TP	Posterior_point_of_the_superior_plate_of_L5	LMK_L5UpperRearEnd	
LUSP01BR	Right_point_of_the_inferior_plate_of_L1	LMK_L1LowerRightEnd	
LUSP02BR	Right_point_of_the_inferior_plate_of_L2	LMK_L2LowerRightEnd	

LUSP03BR	Right_point_of_the_inferior_plate_of_L3	LMK_L3LowerRightEnd	
LUSP04BR	Right_point_of_the_inferior_plate_of_L4	LMK_L4LowerRightEnd	
LUSP05BR	Right_point_of_the_inferior_plate_of_L5	LMK_L5LowerRightEnd	
LUSP01TR	Right_point_of_the_superior_plate_of_L1	LMK_L1UpperRightEnd	
LUSP02TR	Right_point_of_the_superior_plate_of_L2	LMK_L2UpperRightEnd	
LUSP03TR	Right_point_of_the_superior_plate_of_L3	LMK_L3UpperRightEnd	
LUSP04TR	Right_point_of_the_superior_plate_of_L4	LMK_L4UpperRightEnd	
LUSP05TR	Right_point_of_the_superior_plate_of_L5	LMK_L5UpperRightEnd	

Table 11 Common lumbar spine landmarks and corresponding code according to naming convention

ID accoding to new naming convention	Landmark name	Piper Synonyms	Comments
Lower Extremities			
FEMRLDL0	Lateral_epicondyle_of_left_femur	LLATEPIC, Femur_FLE_L, FEL_L	
FEMRRDL0	Lateral_epicondyle_of_right_femur	RLATEPIC, Femur_FLE_R, FEL_R	
FEMRLDM0	Medial_epicondyle_of_left_femur	LMEDEPIC, Femur_FME_L, FEM_L	
FEMRRDM0	Medial_epicondyle_of_right_femur	RMEDEPIC, Femur_FME_R, FEM_R	

FEMRLPL0	Lateral_point_on_greater_trochanter_of_the_left_femur	FTC_L, Femur_FTC_L	
FEMRRPL0	Lateral_point_on_greater_trochanter_of_the_right_femur	FTC_R, Femur_FTC_R	
FEMRLPL1	Tip_greater_trochanter_of_left_femur		
FEMRRPL1	Tip_greater_trochanter_of_right_femur		
FEMRLPM0	Left_Femur_Lesser_Trochanter		
FEMRRPM0	Right_Femur_Lesser_Trochanter		
FEMRLPCR	L_Femur_O		
FEMRRPCR	R_Femur_O		
FEMRLDCR	L_Femur_MP_FEM_FEL		
FEMRRDCR	R_Femur_MP_FEM_FEL		
FEMRLPCR	Head_center_of_left_femur	head_center_femur_L, Femur_FCH_L	
FEMRRPCR	Head_center_of_right_femur	head_center_femur_R, Femur_FCH_R	
FEMRLDXX	Midpoint_of_intercondylar_line_of_the_left_femur		
FEMRRDXX	Midpoint_of_intercondylar_line_of_the_right_femur		
TIBILDXX	L_Tibia_IC		
TIBIRDXX	R_Tibia_IC		
TIBILPL0	Lateral_point_lateral_condyle_of_left_tibia	Lateral_point_lateral_condyle_of_tibia_L, LC_L	
TIBIRPL0	Lateral_point_lateral_condyle_of_right_tibia	Lateral_point_lateral_condyle_of_tibia_R, LC_R	
TIBILPM0	Medial_point_medial_condyle_of_left_tibia	LTIMEDPLAT, Medial_point_medial_condyle_of_tibia_L, MC_L	

TIBIRPM0	Medial_point_medial_condyle_of_right_tibia	RTIMEDPLAT, Medial_point_medial_condyle_of_tibia_R, LMK_RTIMEDPLAT, MC_R	
TIBILPRX	Posterior_intercondylar_area_of_the_left_tibia		
TIBIRPRX	Posterior_intercondylar_area_of_the_right_tibia		
TIBILPFX	Left_tibial_tuberosity		
TIBILPFX	Right_tibial_tuberosity	RTIATUB, tibial_tuberosity_R, Tibia_TTC_R, TT_R	
TIBILDM0	Tip_medial_malleolus_of_left_tibia	Apex_of_the_medial_malleolus_of_the_left_tibia, Tip_medial_malleolus_of_tibia_L, Tibia_TAM_L, MM_L	
TIBIRDM0	Tip_medial_malleolus_of_right_tibia	Apex_of_the_medial_malleolus_of_the_right_tibia, Tip_medial_malleolus_of_tibia_R, Tibia_TAM_R, MM_R	
TIBILPCR	knee_joint_tibia_L		
TIBIRPCR	knee_joint_tibia_R		
FIBULDL0	Tip_lateral_malleolus_of_left_fibula	Tip_lateral_malleolus_of_fibula_L, FAL_L	
FIBULDL1	Tip_lateral_malleolus_of_left_fibula_on_skin	Tip_lateral_malleolus_of_fibula_L_onSkin, FAL_L_onSkin, LM_L	

FIBURDL0	Tip_lateral_malleolus_of_right_fibula	Tip_lateral_malleolus_of_fibula_R, FAL_R	
FIBURDL1	Tip_lateral_malleolus_of_right_fibula_on_skin	Tip_lateral_malleolus_of_fibula_R_onSkin, FAL_R_onSkin, LM_R	
FIBULP00	Apex_of_the_styloid_process_of_the_left_fibula	FAX_L, Fibula_FAX_L	
FIBURP00	Apex_of_the_styloid_process_of_the_right_fibula	FAX_R, Fibula_FAX_R	
ANKLL0CR	L_Malleolus_IM		
ANKLR0CR	R_Malleolus_IM		
FIBULDL0	L_Malleolus_LM		
FIBURDL0	R_Malleolus_LM		
TIBILDM0	L_Malleolus_MM		
TIBIRDM0	R_Malleolus_MM		
HEELL0CG	L_Calcaneus_COG		
HEELR0CG	R_Calcaneus_COG		
HEELLR00	L_Calcaneus_posterior		
HEELRR00	R_Calcaneus_posterior		
HEELLXRL	Center_of_lateral_edge_of_posterior_surface_of_left_calcaneus	FCL_L	
HEELRXRL	Center_of_lateral_edge_of_posterior_surface_of_right_calcaneus	FCL_R	
HEELLXRM	Center_of_medial_edge_of_posterior_surface_of_left_calcaneus	FCM_L	
HEELRXRM	Center_of_medial_edge_of_posterior_surface_of_right_calcaneus	FCM_R	
HEELLXRX	Center_of_posterior_calcaneal_face_of_left_foot	FCC_L	

HEELRXRX	Center_of_posterior_calcaneal_face_of_right_foot	FCC_R	

Table 12 Common landmarks of the lower extremities and corresponding code according to naming convention

ID accoding to new naming convention	Landmark name	Piper Synonyms	Comments
Pelvis			
ACTBL0CR	Left_acetabular_center	LHJCPEL, Cotyle_L, Ilium_IAC_L	
ACTBR0CR	Right_acetabular_center		
ILACLIF0	Left_anterior_inferior_iliac_spine	LAIIS, anterior_inferior_iliac_spine_L	
ILACRIF0	Right_anterior_inferior_iliac_spine	RAIIS, anterior_inferior_iliac_spine_R	
ILACLSF0	L_ASIS	LASIS, anterior_superior_iliac_spine_L, Ilium_IAS_L, ASIS_L	
ILACRSF0	R_ASIS	RASIS, anterior_superior_iliac_spine_R, Ilium_IAS_R, ASIS_R	
ILACLSR0	L_PSIS	LPSIS, posterior_superior_iliac_spine_L, Ilium_IPS_L, PSIS_L	
ILACRSR0	R_PSIS	RPSIS, posterior_superior_iliac_spine_R, Ilium_IPS_R, PSIS_R	

ILACLIR0	Posterior_Inferior_Iliac_Spine_L	LMK_IPI_L, Posterior_Inferior_Iliac_Spine_Left	
ILACRIR0	Posterior_Inferior_Iliac_Spine_R	LMK_IPI_R, Posterior_Inferior_Iliac_Spine_Right	
HPNTX000	H-point		
PUBCX0CE	Pubic Symphysis	LMK_IPJ_M, Ilium_IPJ	
PUBCLM00	Pubic_symphysis_of_the_left_hip	LMK_IPJ_L	
PUBCRM00	Pubic_symphysis_of_the_right_hip	LMK_IPJ_R	
PUBCLSF0	Left Pubic Tubercle		
PELVXIR0	Cocyx_inferior		
SACRXF00	Sacrum_anterior		
SACRXR00	Sacrum_posterior		
SACRXTXX	Center_Sacral_Plate	Center_Sacral_Plate	
SACRXTF0	Anterior_point_of_the_sacral_plate	VS, Most_anterior_point_sacral_plate	
SACRXTR0	Posterior_point_of_the_sacral_plate	DS, Most_posterior_point_sacral_plate	
SACRXIR0	Sacral_hiatus	Sacral_hiatus	
SACR02PP	Spinous_process_of_second_sacral_vertebra	Spinous_process_of_second_sacral_vertebra	
PELVLI00	L_Ischium_inferior		
PELVRI00	R_Ischium_inferior		
ILACLSL0	Crest_tubercle_L	LMK_ICT_L, Crest_tubercle_Left	

ILACRSL0	Crest_tubercle_R	LMK_ICT_R, Crest_tubercle_Right	
PUBCLSFL	Ilium_IPP_L	Ilium_pubic_spine_left	
PUBCRSFL	Ilium_IPP_R	Ilium_pubic_spine_right	
HPNT0000	REF_MP_acetabulum_centers		

Table 13 Common landmarks of the pelvis and corresponding code according to naming convention